DC Optimal Power Flow Formulation and Solution Using QuadProgJ*

Junjie Sun† and Leigh Tesfatsion‡

ISU Economics Working Paper No. 06014
Revised: 1 March 2010

Abstract

Nonlinear AC Optimal Power Flow (OPF) problems are commonly approximated by linearized DC OPF problems to obtain real power solutions for restructured wholesale power markets. We first present a standard DC OPF problem, which has the numerically desirable form of a strictly convex quadratic programming (SCQP) problem when voltage angles are eliminated by substitution. We next augment this standard DC OPF problem in a physically meaningful way, still retaining an SCQP form, so that solution values for voltage angles and locational marginal prices are directly obtained along with real power injections and branch flows. We then show how this augmented DC OPF problem can be solved using *QuadProgJ*, an open-source Java SCQP solver newly developed by the authors that implements the well-known dual active-set SCQP algorithm by Goldfarb and Idnani (1983). To demonstrate the accuracy of QuadProgJ, comparative results are reported for a well-known suite of numerical QP test cases with up to 1500 decision variables plus constraints. Detailed QuadProgJ results are also reported for 3-node and 5-node DC OPF test cases taken from power systems texts and ISO-NE/PJM training manuals.

Keywords: AC optimal power flow, DC OPF approximation, Strictly convex quadratic programming, Dual active-set method; Lagrangian augmentation, Java implementation, QuadProgJ, AMES Market Package

JEL classifications: C61, C63, C88

*This work has been supported in part by the National Science Foundation under Grant NSF-0527460. The authors are grateful to Deddy Koesrindartoto for dedicated collaboration on earlier phases of this project. The authors also thank Donald Goldfarb, William Hogan, Daniel Kirschen, Chen-Ching Liu, Jim McCalley, Michael J. D. Powell, Jim Price, Harold Salazar, Johnny Wong, and Tong Wu for helpful conversations on topics related to this study.

†Starting July 9, 2007, Junjie Sun will assume the position of Financial Economist with the Office of the Comptroller of the Currency, U.S. Treasury, Washington D.C.

‡Corresponding Author: Leigh Tesfatsion (tesfatsi@iastate.edu) is Professor of Economics and Mathematics at Iowa State University, Ames, IA 50011-1070.

1 Introduction

The standard AC Optimal Power Flow (OPF) problem involves the minimization of total variable generation costs subject to nonlinear balance, branch flow, and production constraints for real and reactive power; see Wood and Wollenberg (1996, Chpt. 13). In practice, AC OPF problems are typically approximated by a more tractable "DC OPF" problem that focuses exclusively on real power constraints in linearized form.

We first present a standard DC OPF problem in per unit form. This standard problem can be represented as a *strictly convex quadratic programming (SCQP)* problem, that is, as the minimization of a positive definite quadratic form subject to linear constraints. An SCQP problem can be expressed in matrix form as follows:

Minimize

$$\mathbf{f(x)} = \frac{\mathbf{1}}{\mathbf{2}}\mathbf{x^T G x} + \mathbf{a^T x} \tag{1}$$

with respect to

$$\mathbf{x} \;=\; (\mathbf{x_1}, \mathbf{x_2}, \ldots, \mathbf{x_M})^{\mathbf{T}} \tag{2}$$

subject to

$$\mathbf{C_{eq}^T x} = \mathbf{b_{eq}} \tag{3}$$

$$\mathbf{C_{iq}^T x} \geq \mathbf{b_{iq}} \tag{4}$$

where $\mathbf{G}$ is an $\mathbf{M} \times \mathbf{M}$ symmetric[1] positive definite matrix.

As will be clarified below, the solution of this standard DC OPF problem as an SCQP problem directly provides solution values for real power injections. However, solution values for locational marginal prices (LMPs), voltage angles, and real power branch flows have to be recovered indirectly by additional manipulations of these solution values.

We next show how this standard DC OPF problem can be augmented in a physically meaningful way, still retaining an SCQP form, so that solution values for LMPs, voltage angles, and voltage angle differences are directly recovered along with solution values for real power injections and branch flows. We then carefully explain how this augmented SCQP problem can be solved using *QuadProgJ*, an SCQP solver newly developed by the authors. QuadProgJ implements the well-known dual active-set SCQP algorithm by Goldfarb and Idnani (1983) and appears to be the first open-source SCQP solver developed completely in Java. It is designed for the fast and efficient desktop solution of small to medium-scale SCQP problems for research and training purposes.

More precisely, we show how the augmented DC OPF problem in SCQP form can be solved using QuadProgJ optionally coupled with an outer Java shell (DCOPFJ). This outer shell automatically converts input data from standard SI units to per unit (pu), puts this pu data into the matrix form required by QuadProgJ, and then converts the pu output

[1]Symmetry is assumed here without loss of generality. Since $x^T G x = x^T G^T x$, the matrix G in (1) can always be replaced by the symmetric matrix $\bar{G} = [G + G^T]/2$.

back into SI units. To demonstrate the accuracy of QuadProgJ, we report comparative findings for a well-known suite of numerical QP test cases with up to 1500 decision variables plus constraints. As a test of DCOPFJ coupled with QuadProgJ, we also present detailed numerical findings for illustrative three-node and five-node DC OPF test cases taken from power systems texts and ISO-NE/PJM training manuals.

Section 2 presents the basic configuration of a restructured wholesale power market operating over an AC transmission grid, making use of a computational framework developed by the authors in previous studies. Section 3 carefully derives a standard DC OPF problem in per unit form for this wholesale power market and discusses how this standard formulation can be usefully augmented to enable the direct generation of solution values for LMPs, voltage angles, voltage angle differences, real power injections, and branch flows. Section 4 explicitly derives and presents a complete matrix SCQP representation for this augmented DC OPF problem. Section 5 illustrates this representation for three-node and five-node DC OPF test cases.

Section 6 then explains how the augmented DC OPF problem in SCQP form can be solved using QuadProgJ optionally coupled with the DCOPFJ shell. Section 7 reports comparative QP test case results, and Section 8 presents detailed numerical findings for the three-node and five-node DC OPF test cases. Concluding remarks are given in Section 9. Technical notes on the derivation of AC power flow equations from Ohm's Law and on the SCQP representation of the standard DC OPF problem are provided in appendices.

2 Configuration of the Wholesale Power Market

Formulation of DC OPF problems for restructured wholesale power markets requires detailed structural information about the transmission grid as well as supply offer and demand bid information for market participants. This section briefly but carefully describes a computational framework ("AMES") previously developed by the authors for the dynamic study of restructured wholesale power markets. The following Section 3 then sets out a standard DC OPF problem based on this wholesale power market framework.

2.1 Overview of the AMES Framework

In April 2003 the U.S. Federal Energy Regulatory Commission proposed a *Wholesale Power Market Platform (WPMP)* for common adoption by all U.S. wholesale power markets (FERC, 2003). In a series of previous studies[2] we have developed a Java framework modeling a restructured wholesale power market operating over an AC transmission grid in accordance with core features of the WPMP as implemented by the ISO New England in its Standard Market Design (ISO-NE, 2003) and by the Midwest ISO in its April 2005 market initiative (MISO, 2007).

This framework – referred to as *AMES*[3] – includes an Independent System Operator (ISO) and a collection of bulk energy traders consisting of Load-Serving Entities (LSEs)

[2]See Koesrindartoto and Tesfatsion (2004), Koesrindartoto et al. (2005), and Sun and Tesfatsion (2007).
[3]AMES is an acronym for *A*gent-based *M*odeling of *E*lectricity *S*ystems.

and Generators distributed across the nodes of the transmission grid.[4] In general, multiple Generators at multiple nodes could be under the control of a single generation company ("GenCo"), and similarly for LSEs. This control aspect is critically important to recognize for the study of strategic trading, but it plays no role in the current study.

The AMES ISO undertakes the daily operation of the transmission grid within a two-settlement system using *Locational Marginal Pricing*.[5] More precisely, at the beginning of each operating day D the AMES ISO determines hourly power commitments and *Locational Marginal Prices (LMPs)*[6] for the day-ahead market for day $D+1$ based on Generator supply offers and LSE demand bids (forward financial contracting). Any differences that arise during day $D+1$ between real-time conditions and the contracts cleared and settled in day D for the day-ahead market for $D+1$ are settled by the AMES ISO in the real-time market for $D+1$ at real-time LMPs. Transmission grid congestion is managed by the inclusion of congestion components in LMPs.

As discussed more carefully in Sections 2.3 and 2.4 below, the current study makes the usual empirically-based assumption that the daily demand bids of the AMES LSEs exhibit negligible price sensitivity and hence reduce to daily load profiles. In addition, it is assumed for notational simplicity that the AMES Generators submit supply offers consisting of their true marginal cost functions and true production limits (i.e., they do not make strategic offers). In this case the optimization problem faced by the ISO for each hour of the day-ahead market reduces to a standard AC OPF problem requiring the minimization of (true) total variable generation costs subject to balance constraints, branch flow constraints, (true) production constraints, and given loads. As is commonly done in practice, the AMES ISO approximates this nonlinear AC OPF problem by means of a DC OPF problem with linearized constraints. The AMES ISO invokes QuadProgJ through the DCOPFJ shell in order to solve this DC OPF problem in per unit form.

The remainder of this section explains the configuration of the AMES transmission grid and market participants.

[4] An *Independent System Operator (ISO)* is an organization charged with the primary responsibility of maintaining the security of a power system and often with system operation responsibilities as well. The ISO is "independent" to the extent that it does not have a conflict of interest in carrying out these responsibilities, such as an ownership stake in generation or transmission facilities within the power system. A *Load-Serving Entity (LSE)* is an electric utility, transmitting utility, or Federal power marketing agency that has an obligation under Federal, State, or local law, or under long-term contracts, to provide electrical power to end-use (residential or commercial) consumers or to other LSEs with end-use consumers. An LSE aggregates individual end-use consumer demand into "load blocks" for bulk buying at the wholesale level. A *Generator* is a unit that produces and sells electrical power in bulk at the wholesale level. A *node* is a point on the transmission grid where power is injected or withdrawn.

[5] *Locational Marginal Pricing* is the pricing of electrical power according to the location of its withdrawal from, or injection into, a transmission grid.

[6] A *Locational Marginal Price (LMP)* at any particular node of a transmission grid is the least cost of meeting demand for one additional unit (MW) of power at that node.

2.2 Configuration of the AMES Transmission Grid

The AMES transmission grid is an alternating current (AC) grid modeled as a balanced three-phase network with $N \geq 1$ branches and $K \geq 2$ nodes. Reactances on branches are assumed to be total reactances (rather than per mile reactances), meaning that branch length is already taken into account. All transformer phase angle shifts are assumed to be zero, all transformer tap ratios are assumed to be 1, all line-charging capacitances are assumed to be 0, and the temperature is assumed to remain constant over time.

The AMES transmission grid is assumed to be *connected* in the sense that it has no isolated components; each pair of nodes k and m is connected by a linked branch path consisting of one or more branches. If two nodes are in direct connection with each other, it is assumed to be through at most one branch, i.e., branch groups are not explicitly considered. However, complete connectivity is *not* assumed, that is, node pairs are *not* necessarily in direct connection with each other through a single branch.

For per unit normalization in DC OPF implementations, it is conventional to specify base value settings for apparent power (voltampere) and voltage.[7] For the AMES transmission grid, the base apparent power, denoted by S_o, is assumed to be measured in three-phase megavoltamperes (MVAs), and the base voltage, denoted by V_o, is assumed to be measured in line-to-line kilovolts (kVs).

It is also assumed that *Kirchoff's Current Law (KCL)* governing current flows in electrical networks holds for the AMES transmission grid for each hour of operation. As detailed in Kirschen and Strbac (2004, Section 6.2.2.1), KCL implies that real and reactive power must each be in balance at each node. Thus, real power must also be in balance across the entire grid, in the sense that aggregate real power withdrawal plus aggregate transmission losses must equal aggregate real power injection.

In wholesale power markets restructured in accordance with FERC's proposed WPMP market design (FERC, 2003), the transmission grid is overlaid with a commercial network consisting of "pricing locations" for the purchase and sale of electric power. A *pricing location* is a location at which market transactions are settled using publicly available LMPs. For simplicity, it is assumed that the set of pricing locations for AMES coincides with the set of transmission grid nodes.

2.3 Configuration of the AMES LSEs

The AMES LSEs purchase bulk power in the AMES wholesale power market in order to service customer demand (load) in a downstream retail market. The user specifies the number J of LSEs as well as the location of these LSEs at various nodes of the transmission grid. LSEs do not engage in production or sale activities in the wholesale power market. Hence, LSEs purchase power only from Generators, not from each other.

At the beginning of each operating day D, each AMES LSE j submits a *daily load profile* into the day-ahead market for day $D + 1$. This daily load profile indicates the real power demand $p_{Lj}(H)$ that must be serviced by LSE j in its downstream retail market for each of 24

[7] For a detailed and careful discussion of base value determinations and per unit calculations for power system applications, see Anderson (1995, Chpt. 1) and Gönen (1988, Chpt. 2).

successive hours H. In the current AMES modeling, the standard assumption is made that these demands are not price sensitive. One possible interpretation of this price-insensitivity assumption is that the AMES LSEs are required by retail regulations to service their load profiles as "native"[8] load obligations, and that the profit (revenues net of costs) received by LSEs for servicing these load obligations is regulated to be a simple dollar mark-up over cost that is independent of the cost level. Under these conditions, LSEs have no incentive to submit price-sensitive demand bids into the day-ahead market.

2.4 Configuration of the AMES Generators

The Ames Generators are electric power generating units. The user specifies the number I of Generators as well as the location of these Generators at various nodes of the transmission grid. Generators sell power only to LSEs, not to each other.

Each AMES Generator is user-configured with technology, endowment, and learning attributes. Only the technology attributes are relevant for the current study. With regard to the latter, it is assumed that each Generator has variable and fixed costs of production. However, Generators do not incur no-load, startup, or shutdown costs, and they do not face ramping constraints.[9]

More precisely, the technology attributes assumed for each Generator i take the following form. Generator i has minimum and maximum capacities for its hourly real power production level p_{Gi} (in MWs), denoted by p^L_{Gi} and p^U_{Gi}, respectively.[10] That is, for each i,

$$p^L_{Gi} \;\leq\; p_{Gi} \;\leq\; p^U_{Gi} \tag{5}$$

In addition, Generator i has a *total cost function* giving its total costs of production per hour for each hourly production level p. This total cost function takes the form

$$\mathrm{TC}_i(p) \;=\; a_i \cdot p \;+\; b_i \cdot p^2 \;+\; \mathrm{FCost}_i \tag{6}$$

where a_i (\$/MWh), b_i (\$/MW^{2}h), and FCost_i (\$/h) are exogenously given constants. Note that $\mathrm{TC}_i(p)$ is measured in dollars per hour (\$/h). Generator i's *total variable cost function* and *(prorated) fixed costs* for any feasible hourly production level p are then given by

$$\mathrm{TVC}_i(p) \;=\; \mathrm{TC}_i(p) - \mathrm{TC}_i(0) \;=\; a_i \cdot p \;+\; b_i \cdot p^2 \tag{7}$$

[8]Native load customers for an LSE are customers whose power needs the LSE is obliged to meet by statute, franchise, regulatory requirement, or contract.

[9]As is standard in economics, *variable costs* are costs that vary with the level of production, and *fixed costs* are costs such as debt and equity obligations associated with plant investments that are not dependent on the level of production and that are incurred even if production ceases. As detailed by Kirschen and Strbac (2004, Section 4.3), the concept of *no-load costs* in power engineering refers to *quasi-fixed* costs that would be incurred by Generators if they could be kept running at zero output but that would vanish once shut-down occurs. *Startup costs* are costs specifically incurred when a Generator starts up, and *shutdown costs* are costs specifically incurred when a Generator shuts down. Finally, *ramping constraints* refer to physical restrictions on the rates at which Generators can increase or decrease their outputs.

[10]In the current AMES modeling, the lower production limit p^L_{Gi} for each Generator i is interpreted as a firm "must run" minimum power production level. That is, if p^L_{Gi} is positive, then shutting down Generator i is not an option for the AMES ISO. Consequently, for most applications of AMES, these lower production limits should be set to zero.

and

$$\text{FCost}_i \;=\; \text{TC}_i(0) \tag{8}$$

respectively. Finally, the *marginal cost function* for Generator i takes the form

$$\text{MC}_i(p) \;=\; a_i \;+\; 2 \cdot b_i \cdot p \tag{9}$$

At the beginning of each operating day D, each Generator i submits a *supply offer* into the day-ahead market for use in each hour H of day $D+1$. This supply offer consists of a reported marginal cost function defined over a reported feasible production interval. In general, this supply offer could be strategic in the sense that the reported marginal cost function deviates from Generator i's true marginal cost function $MC_i(p)$ and the reported feasible production interval differs from Generator i's true feasible production interval $[p^L_{Gi}, p^U_{Gi}]$. For the purposes of this paper, however, it can be assumed without loss of generality that each Generator i reports its true marginal cost function and its true feasible production interval.[11]

3 DC OPF Problem Formulation

A DC OPF problem is an approximation for an underlying AC OPF problem under several simplifying restrictions regarding voltage magnitudes, voltage angles, admittances, and reactive power. To lessen the chances of numerical instability, the variables appearing in the resulting DC OPF problem are commonly expressed in normalized *per unit (pu)* values so that the magnitudes of these variables are more nearly equal to each other.[12] In Section 3.1 we briefly but carefully outline the manner in which a standard DC OPF problem *expressed in pu values* is derived from an underlying AC OPF problem expressed in standard SI (International System of Units).

Using the results of Section 3.1, we then derive in Section 3.2 a standard DC OPF problem in full structural pu form for the AMES wholesale power market set out in Section 2. In particular, we show that this problem can be expressed as a strictly convex quadratic programming (SCQP) problem once voltage angles are eliminated by substitution from the problem constraints. An SCQP formulation is highly desirable from the standpoint of stable numerical solution. Unfortunately, this voltage angle substitution eliminates the nodal balance constraints and hence the ability to directly generate solution values for LMPs, which by definition are the shadow prices for the nodal balance constraints.

[11] Thus, the Generators' supply offers take the form of linear upward-sloping supply curves. As detailed in Sun and Tesfatsion (2007), this representation for supply offers greatly facilitates the modeling of Generator learning. In the actual ISO-NE and MISO wholesale power markets, generators submit their supply offers in the form of non-decreasing step functions (MW/price blocks) defined over their feasible production intervals. However, with generator permission, the ISO uses the step points to construct smoothed offer approximations.

[12] As will be clarified in subsequent sections, QuadProgJ can directly accept DC OPF variable inputs expressed in pu form so that all internal calculations are carried out in pu terms. Alternatively, as explained in Section 6, QuadProgJ can be coupled with an outer DCOPFJ shell that automatically converts wholesale power market variables from standard SI to per unit form prior to invoking QuadProgJ.

Consequently, in Sections 3.3 and 3.4 we develop an alternative version of this standard DC OPF problem in pu form making use of a physically meaningful Lagrangian augmentation. This augmented DC OPF problem directly generates solution values for LMPs, voltage angles, and voltage angle differences as well as real power injections and branch flows while still retaining a numerically desirable SCQP form.

3.1 From AC OPF to DC OPF Per Unit

Conversion of an AC OPF problem to a DC OPF approximation in per unit form requires careful attention to variable conversions in both the problem constraints and the problem objective function. Here we first consider constraint conversions and then take up the needed conversions for the objective function.

The key constraints in an AC OPF problem that are simplified in a DC OPF approximation are the representations for real and reactive power branch flows. Let km denote a branch that connects nodes k and m with $k \neq m$. Let P_{km} (in MWs) denote the real power branch flow for km, and let Q_{km} (in MVARs) denote the reactive power branch flow for km. Let V_k and V_m denote the voltage magnitudes (in kVs) at nodes k and m, and let δ_k and δ_m denote the voltage angles (in radians) at nodes k and m. Finally, let g_{km} and b_{km} denote the conductance and the susceptance (in mhos) for branch km.[13]

Given these notational conventions, P_{km} and Q_{km} ($k \neq m$) can be expressed as follows:[14]

$$P_{km} = V_k^2 g_{km} - V_k V_m [g_{km} \cos(\delta_k - \delta_m) + b_{km} \sin(\delta_k - \delta_m)] \tag{10}$$

$$Q_{km} = -V_k^2 b_{km} - V_k V_m [g_{km} \sin(\delta_k - \delta_m) - b_{km} \cos(\delta_k - \delta_m)] \tag{11}$$

The three basic assumptions used to derive a DC OPF approximation from an underlying AC OPF problem are as follows (c.f. Kirschen and Strabac, 2004, p. 186, and McCalley, 2006):

[A1] The resistance r_{km} for each branch km is negligible compared to the reactance x_{km} and can therefore be set to 0.

[A2] The voltage magnitude at each node is equal to the base voltage V_o.

[A3] The voltage angle difference $\delta_k - \delta_m$ across any branch km is sufficiently small in magnitude so that $\cos(\delta_k - \delta_m) \approx 1$ and $\sin(\delta_k - \delta_m) \approx [\delta_k - \delta_m]$.

Given assumption [A1], it follows that $g_{km} = 0$ and $b_{km} = [-1/x_{km}]$, where x_{km} denotes the reactance (in ohms) for branch km. Thus, $P_{km} = V_k V_m [1/x_{km}] \sin(\delta_k - \delta_m)$ and $Q_{km} =$

[13] *Impedance* takes the complex form $z = r + \sqrt{-1}\, x$, where r (in ohms) denotes resistance and x (in ohms) denotes reactance. *Admittance* (the inverse of impedance) then takes the complex form $y = g + \sqrt{-1}\, b$, where the *conductance* is given by $g = r/[r^2 + x^2]$ (in mhos) and the *susceptance* is given by $b = -x/[r^2 + x^2]$ (in mhos).

[14] See Appendix A for a rigorous derivation of these power flow equations from Ohm's Law.

$V_k^2[1/x_{km}] - V_k V_m[1/x_{km}]\cos(\delta_k - \delta_m)$. Adding assumption [A2], $P_{km} = V_o^2[1/x_{km}]\sin(\delta_k - \delta_m)$ and $Q_{km} = V_o^2[1/x_{km}] - V_o^2[1/x_{km}]\cos(\delta_k - \delta_m)$. Finally, adding assumption [A3],

$$P_{km} \;=\; V_o^2 \cdot [1/x_{km}] \cdot [\delta_k - \delta_m] \tag{12}$$

and the reactive power branch flow Q_{km} in equation (11) reduces to $Q_{km} = V_o^2[1/x_{km}] - V_o^2[1/x_{km}] \cdot 1 = 0$.

As detailed in Anderson (1995, Chpt. 1) and Gönen (1988, Chpt. 2), any quantity in an electrical network can be converted to a dimensionless pu quantity by dividing its numerical value by a base value of the same dimension. In power system calculations, only two base values are needed; and these are usually taken to be base voltage and base apparent power (voltampere). Assuming a balanced three-phase network with a base voltage V_o measured in line-to-line kVs and a base apparent power S_o measured in three-phase MVAs, the *base impedance* Z_o (in ohms) is specified to be

$$Z_o \;=\; V_o^2/S_o \tag{13}$$

Given Z_o, the *pu reactance* x_{km} for branch km is defined to be

$$x_{km} \;\text{ pu} \;=\; x_{km}/Z_o \tag{14}$$

Note that x_{km} pu is a dimensionless quantity. Using assumption [A3], the *pu susceptance* b_{km} for branch km is given by

$$b_{km} \;\text{ pu} \;=\; -\,1/[x_{km} \text{ pu}] \tag{15}$$

Also, the *pu real power branch flow* F_{km} for branch km is given by

$$F_{km} \;=\; P_{km}/S_o \tag{16}$$

Now divide each side of the real power branch flow equation (12) by the base apparent power S_o. Also, let B_{km} denote the negative of the susceptance pu on branch km. That is, define

$$B_{km} \;=\; -\,b_{km} \;\text{ pu} \;=\; [1/x_{km} \text{ pu}] \tag{17}$$

It then follows from equations (13) through (17) that the real power branch flow equation (12) can be expressed in the following simple linear pu form commonly seen in power systems textbooks:

$$F_{km} \;=\; B_{km}[\delta_k - \delta_m] \tag{18}$$

As will be clarified below, an additional change of variables needed to express the DC OPF problem in pu terms is to everywhere divide real power quantities by base apparent power S_o. Thus, for example, the real power p_{Gi} injected by each Generator i is expressed in pu terms as

$$P_{Gi} \;=\; p_{Gi}/S_o \tag{19}$$

and the real power load p_{Lj} withdrawn by each LSE j is expressed in pu terms as

$$P_{Lj} \;=\; p_{Lj}/S_o \tag{20}$$

The objective function for the DC OPF problem must be expressed in pu terms as well as the constraints. Thus, the total cost function and variable cost function defined in Section 2.4 for each Generator i are expressed as a function of pu real power P_{Gi} as follows:

$$\mathrm{TC}_i(P_{Gi}) \;=\; A_i \cdot P_{Gi} \;+\; B_i \cdot P_{Gi}^2 \;+\; \mathrm{FCost}_i \tag{21}$$

$$\mathrm{TVC}_i(P_{Gi}) \;=\; A_i \cdot P_{Gi} \;+\; B_i \cdot P_{Gi}^2 \tag{22}$$

where A_i (\$/h) and B_i (\$/h) are pu-adjusted cost coefficients defined by

$$A_i = a_i S_o \tag{23}$$

$$B_i = b_i S_o^2 \tag{24}$$

Note that the pu-adjusted cost functions $\mathrm{TC}_i(P_{Gi})$ and $\mathrm{TVC}_i(P_{Gi})$ are still measured in dollars per hour (\$/h).

Finally, as usual, one node needs to be selected as the reference node with a specified voltage angle. For concreteness, we make the following assumption:

[A4] Node 1 is the reference node with voltage angle normalized to 0.

3.2 Standard DC OPF in Structural PU Form

This subsection sets out a standard DC OPF problem for the AMES wholesale power market in full structural pu form, making use of the developments in Section 3.1. It is then seen that this standard problem can be expressed in numerically desirable SCQP form if the voltage angles are eliminated by substitution from the problem constraints.

For easy reference, the admissible exogenous variables and endogenous variables used in the standard DC OPF formulation are gathered together in Tables 1 and 2, respectively. These variable definitions will be used throughout the remainder of this study.

Given the variable definitions in Tables 1 and 2, the standard DC OPF problem for the AMES wholesale power market formulated in pu terms is as follows:

Minimize

$$\sum_{i=1}^{I} [A_i P_{Gi} + B_i P_{Gi}^2] \tag{25}$$

with respect to

$$P_{Gi},\ i = 1, ..., I; \quad \delta_k,\ k = 1, ..., K$$

subject to:

Real power balance constraint for each node $\mathbf{k = 1, ..., K}$:

Table 1: DC OPF Admissible Exogenous Variables Per Unit

Variable	Description	Admissibility Restrictions
K	Total number of transmission grid nodes	$K > 0$
N	Total number of distinct network branches	$N > 0$
I	Total number of Generators	$I > 0$
J	Total number of LSEs	$J > 0$
I_k	Set of Generators located at node k	$\text{Card}(\cup_{k=1}^{K} I_k) = I$
J_k	Set of LSEs located at node k	$\text{Card}(\cup_{k=1}^{K} J_k) = J$
S_o	Base apparent power (in three-phase MVAs)	$S_o \geq 1$
V_o	Base voltage (in line-to-line kVs)	$V_o > 0$
V_k	Voltage magnitude (in kVs) at node k	$V_k = V_o,\ k = 1, \ldots, K$
P_{Lj}	Real power load (pu) withdrawn by LSE j	$P_{Lj} \geq 0,\ j = 1, \ldots, J$
km	Branch connecting nodes k and m (if one exists)	$k \neq m$
BR	Set of all distinct branches km, $k < m$	$BR \neq \emptyset$
x_{km}	Reactance (pu) for branch km	$x_{km} = x_{mk} > 0,\ km \in BR$
B_{km}	$[1/x_{km}]$ for branch km	$B_{km} = B_{mk} > 0,\ km \in BR$
F_{km}^{U}	Thermal limit (pu) for real power flow on km	$F_{km}^{U} > 0,\ km \in BR$
δ_1	Reference node 1 voltage angle (in radians)	$\delta_1 = 0$
P_{Gi}^{L}	Lower real power limit (pu) for Generator i	$P_{Gi}^{L} \geq 0,\ i = 1, \ldots, I$
P_{Gi}^{U}	Upper real power limit (pu) for Generator i	$P_{Gi}^{U} > 0,\ i = 1, \ldots, I$
A_i, B_i	Cost coefficients (pu adjusted) for Generator i	$B_i > 0,\ i = 1, \ldots, I$
FCost_i	Fixed costs (hourly prorated) for Generator i	$\text{FCost}_i \geq 0,\ i = 1, \ldots I$
$\text{MC}_i(P)$	$\text{MC}_i(P) = A_i + 2B_iP$ = Generator i's MC function	$\text{MC}_i(P_{Gi}^{L}) \geq 0,\ i = 1, \ldots I$

Table 2: DC OPF Endogenous Variables Per Unit

Variable	Description
P_{Gi}	Real power injection (pu) by Generator $i = 1, \ldots, I$
δ_k	Voltage angle (in radians) at node $k = 2, \ldots, K$
F_{km}	Real power (pu) flowing in branch $km \in$ BR
PGen_k	Total real power injection (pu) at node $k = 1, \ldots, K$
PLoad_k	Total real power withdrawal (pu) at node $k = 1, \ldots, K$
PNetInject_k	Total net real power injection (pu) at node $k = 1, \ldots, K$

$$0 \;=\; \mathrm{PLoad}_k \;-\; \mathrm{PGen}_k \;+\; \mathrm{PNetInject}_k \tag{26}$$

where

$$\mathrm{PLoad}_k \;=\; \sum_{j \in J_k} P_{Lj} \tag{27}$$

$$\mathrm{PGen}_k \;=\; \sum_{i \in I_k} P_{Gi} \tag{28}$$

$$\mathrm{PNetInject}_k \;=\; \sum_{km \,\mathrm{or}\, mk \in BR} F_{km} \tag{29}$$

$$F_{km} \;=\; B_{km}\,[\delta_k - \delta_m] \tag{30}$$

Real power thermal constraint for each branch km $\in$ BR:

$$|F_{km}| \;\leq\; F_{km}^U \tag{31}$$

Real power production constraint for each Generator i = 1, .., I:

$$P_{Gi}^L \;\leq\; P_{Gi} \;\leq\; P_{Gi}^U \tag{32}$$

Voltage angle setting at reference node 1:

$$\delta_1 \;=\; 0 \tag{33}$$

As it stands, this standard DC OPF problem in pu form is a positive *semi-definite* quadratic programming problem. To see this, recall the general matrix form of a quadratic programming problem depicted in Section 1. The objective function (25) expressed in the quadratic form (1) with $x = (P_{G1}, \ldots, P_{GI}, \delta_1, \ldots, \delta_K)^T$ entails a diagonal matrix G with positive entries in its first I diagonal elements corresponding to the real power injections P_{Gi} but zeroes in its remaining K diagonal elements corresponding to the voltage angles δ_k, implying that G is a positive semi-definite matrix.

As shown in Appendix B, it is possible to use the nodal balance constraints (26) for $k = 2, \ldots, K$ together with the normalization constraint (33) to express the voltage angle vector $(\delta_2, \ldots, \delta_K)$ as a linear affine function of the real power injection vector $(P_{G1}, \ldots, P_{GI})$. Using this relation to everywhere eliminate the voltage angles does result in a numerically more desirable SCQP problem. Unfortunately, this voltage angle elimination also prevents the direct determination of solution values for LMPs since, by definition, the LMPs are the shadow prices for the nodal balance constraints.

The following subsection develops a simple physically meaningful augmentation of the standard DC OPF objective function that permits direct generation of optimal LMPs and voltage angle solutions while retaining a numerically desirable SCQP form.

3.3 Augmentation of the Standard DC OPF Problem

Consider the following augmentation of the standard DC OPF objective function (25) with a soft penalty function on the sum of the squared voltage angle differences:

$$\sum_{i=1}^{I}[A_i P_{Gi} + B_i P_{Gi}^2] \; + \; \pi \left[\sum_{km \in BR} [\delta_k - \delta_m]^2 \right] \tag{34}$$

As demonstrated carefully in Section 4 below, this augmentation transforms the standard DC OPF problem into an SCQP problem that can be used to directly generate solution values for LMPs and voltage angles as well as real power injections and branch flows, a clear benefit. However, this augmentation also has two additional potential benefits based on physical and mathematical considerations:

- *Physical Considerations:* The augmentation provides a way to conduct sensitivity experiments on the size of the voltage angle differences that could be informative for estimating the size and pattern of AC-DC approximation errors.

- *Mathematical Considerations:* The augmentation could help to improve the numerical stability and convergence properties of any applied solution method.

On the other hand, the augmentation would also seem to come with a potential cost. Specifically, could it cause significant distortions in the standard DC OPF solution values?

This subsection takes up each consideration in turn. The bottom line, supported by experimental evidence, is that solution distortions appear to be practically controllable to arbitrarily small levels through appropriately small settings of the soft penalty weight π. Consequently, the benefits of augmentation would seem to strongly outweigh the costs.

3.3.1 Potential Benefits Based on Physical Considerations

The standard DC OPF problem in pu form set out in Section 3.2 requires the minimization of total variable costs subject to a set of linearized constraints. As detailed in Section 3.1, this pu form relies on the four simplifying assumptions [A1] through [A4]. In particular, the linear form of the branch flow constraints relies on assumption [A3] asserting that voltage angle differences across branches remain small.

Consequently, small voltage angle differences is the basis upon which a DC approximation to a true underlying AC OPF problem is formulated. Nevertheless, the standard DC OPF problem does not constrain voltage angle differences apart from the constraints imposed through branch flow limits, a conceptually distinct type of constraint motivated in terms of the physical attributes of transmission lines. If the presumption of small voltage angle differences is violated, the errors induced by reliance on a DC approximation could become unacceptably large.

Much remains to be done regarding how small is small enough for voltage angle differences in order to achieve satisfactory DC OPF approximations not only for AC OPF quantity solutions (real power injections and branch flows) but also for AC OPF price solutions (the

LMP at each node). We have only been able to find one study of this issue (Overbye et al., 2004) that takes both quantity and price solutions into account. The conclusions reached by the authors on the basis of two case studies are cautiously optimistic with regard to quantity solutions. However, as the authors note, the LMPs are determined by the binding branch flow constraints, hence small branch flow changes causing changes in the binding branch flow constraints can have discrete and potentially large impacts on LMP solutions. For example, in the authors' second case study, the DC approximation missed almost 50% of the binding constraints for the AC problem. Although many of these were "near misses," the effects of these near-misses on the LMP approximations were in some cases significant.

For these reasons, it would seem prudent to pay close attention to the sizes of the voltage angle differences when undertaking DC OPF approximations to AC OPF problems. DC solutions obtained with large voltage angle differences could diverge significantly from AC solutions, thus giving misleading signals - particularly price signals – for the operation of restructured wholesale power markets.

Introducing a soft penalty function on voltage angle differences permits sensitivity checks to be conducted to determine the sensitivity of DC OPF solutions to impositions of this precondition for AC-DC approximation. Ideally, the DC OPF solutions obtained with sufficiently small soft penalty weights π should reproduce the DC OPF solutions obtained in the absence of any soft penalty imposition, as a baseline for comparison. This is indeed seen to be the case in the numerical π sensitivity results reported in Section 8.4.

3.3.2 Potential Benefits Based on Mathematical Considerations

As is well known, numerical stability and convergence properties of nonlinear programming problems with minimization (maximization) objectives can often be enhanced by increasing the convexity (concavity) of their objective functions through suitable augmentations.

For example, the Fortran package ZQPCVX developed by Powell (1983) for convex QP minimization problems includes a simple artificial augmentation to induce strict convexity. Specifically, the matrix diagonal of the positive semi-definite quadratic form representing the nonlinear part of the objective function is augmented with positively-valued constants to induce positive definiteness. More generally, Shahidehpour et al. (2002, Appendix B.2) discuss an entire class of artificial augmentations suitable for nonlinear programming problems with inequality constraints. The authors use versions of these augmentations on pages 288-289 and elsewhere in their text to improve the convexity (hence the convergence properties) of various types of optimization problems arising for electric power systems.

Although artificial augmentations can work well to ensure stability and convergence, they do not provide meaningful sensitivity information for the physical problem at hand. Happily, as explained above, a physically meaningful augmentation is available for the standard DC OPF problem that accomplishes strict convexification of the objective function with several important side benefits.

3.3.3 Potential Costs in Terms of Solution Distortions

In Section 8.4 we report findings for extensive tests conducted with 3-node and 5-node DC OPF problems to check the extent to which the soft penalty function augmentation affects standard DC OPF solution values. To briefly summarize, these findings indicate that the effects of this augmentation on the resulting solution values are negligible for a sufficiently small setting of the soft penalty weight π. Moreover, no numerical instability or convergence problems were detected for any of the tested π values.

3.4 Augmented DC OPF in Reduced PU Form

The augmented DC OPF problem in structural pu form obtained by replacing the standard DC OPF objective function (25) by the augmented objective function (34) can be compactly represented in the following reduced form:

Minimize

$$\sum_{i=1}^{I}[A_i P_{Gi} + B_i P_{Gi}^2] \; + \pi \left[\sum_{1m \in BR} \delta_m^2 + \sum_{km \in BR, \; k \geq 2} [\delta_k - \delta_m]^2 \right] \tag{35}$$

with respect to

$$P_{Gi}, \; i = 1, ..., I; \quad \delta_k, \; k = 2, ..., K$$

subject to:

Real power balance constraint for each node $\mathbf{k = 1, ..., K}$ (with $\delta_1 \equiv 0$):

$$\sum_{i \in I_k} P_{Gi} - \sum_{km \, \text{or} \, mk \in BR} B_{km}[\delta_k - \delta_m] \; = \; \sum_{j \in J_k} P_{Lj} \tag{36}$$

Real power thermal constraints for each branch $\mathbf{km \in BR}$ (with $\delta_1 \equiv 0$):

$$-B_{km}[\delta_k - \delta_m] \; \geq \; -F_{km}^U \tag{37}$$

$$B_{km}[\delta_k - \delta_m] \; \geq \; -F_{km}^U \tag{38}$$

Real power production constraints for each Generator $\mathbf{i = 1, .., I}$:

$$P_{Gi} \; \geq \; P_{Gi}^L \tag{39}$$

$$-P_{Gi} \; \geq \; -P_{Gi}^U \tag{40}$$

4 Augmented DC OPF in SCQP Form

As a preliminary step towards a SCQP depiction for the augmented DC OPF problem in reduced pu form presented in Section 3.4, it is useful to introduce some notational conventions to simplify the exposition. The next two subsections develop matrix representations for the objective function and constraints. The final subsection then presents the complete SCQP depiction in a matrix form suitable for QuadProgJ solution.

4.1 Objective Function Depiction

Consider, first, the development of a quadratic form representation for the soft penalty function applied to voltage angle differences in the augmented DC OPF objective function (35). As detailed in Section 2.2, care must be taken in this representation to account for the possible lack of direct branch connections between nodes.

To this end, define the *branch connection matrix* $\mathbb{E}$ as follows:

$$\mathbb{E} = \begin{bmatrix} 0 & \mathbb{I}(1 \leftrightarrow 2) & \mathbb{I}(1 \leftrightarrow 3) & \cdots & \mathbb{I}(1 \leftrightarrow K) \\ \mathbb{I}(2 \leftrightarrow 1) & 0 & \mathbb{I}(2 \leftrightarrow 3) & \cdots & \mathbb{I}(2 \leftrightarrow K) \\ \mathbb{I}(3 \leftrightarrow 1) & \mathbb{I}(3 \leftrightarrow 2) & 0 & \cdots & \mathbb{I}(3 \leftrightarrow K) \\ \vdots & \vdots & \vdots & \ddots & \vdots \\ \mathbb{I}(K \leftrightarrow 1) & \mathbb{I}(K \leftrightarrow 2) & \mathbb{I}(K \leftrightarrow 3) & \cdots & 0 \end{bmatrix}_{K \times K} \tag{41}$$

where $\mathbb{I}(\cdot)$ is an indicator function defined as:

$$\mathbb{I}(k \leftrightarrow m) = \begin{cases} 1 & \text{if either } km \text{ or } mk \in BR \\ 0 & \text{otherwise} \end{cases}$$

Since $\mathbb{I}(k \leftrightarrow m) = \mathbb{I}(m \leftrightarrow k)$ for all k and m, it follows that $\mathbb{E}_{km} = \mathbb{E}_{mk}$ for all k and m. Thus, $\mathbb{E}$ is a symmetric matrix.

Using this indicator function construct, the number N of distinct transmission grid branches can be determined as follows:

$$N = \left[\sum_{k,m=1}^{K} \mathbb{I}(k \leftrightarrow m) \right] /2 \tag{42}$$

If the transmission grid is completely connected, then $N = K[K-1]/2$.

Next, define the *(voltage angle difference) weight matrix* $\mathbf{W}(\mathbf{K})$ as

$$\mathbf{W}(\mathbf{K}) = 2\pi \begin{bmatrix} \sum_{k \neq 1} \mathbb{E}_{k1} & -\mathbb{E}_{12} & -\mathbb{E}_{13} & \cdots & -\mathbb{E}_{1K} \\ -\mathbb{E}_{21} & \sum_{k \neq 2} \mathbb{E}_{k2} & -\mathbb{E}_{23} & \cdots & -\mathbb{E}_{2K} \\ -\mathbb{E}_{31} & -\mathbb{E}_{32} & \sum_{k \neq 3} \mathbb{E}_{k3} & \cdots & -\mathbb{E}_{3K} \\ \vdots & \vdots & \vdots & \ddots & \vdots \\ -\mathbb{E}_{K1} & -\mathbb{E}_{K2} & -\mathbb{E}_{K3} & \cdots & \sum_{k \neq K} \mathbb{E}_{kK} \end{bmatrix}_{K \times K} \tag{43}$$

For example, in the special case of a completely connected grid, the weight matrix $\mathbf{W}(\mathbf{K})$ takes the form

$$\mathbf{W}(\mathbf{K}) = 2\pi \begin{bmatrix} K-1 & -1 & -1 & \cdots & -1 \\ -1 & K-1 & -1 & \cdots & -1 \\ -1 & -1 & K-1 & \cdots & -1 \\ \vdots & \vdots & \vdots & \ddots & \vdots \\ -1 & -1 & -1 & \cdots & K-1 \end{bmatrix}_{K \times K} \tag{44}$$

Let $\delta(\mathbf{K})^{\mathbf{T}} = [\delta_1 \dots \delta_K]$ denote an arbitrary K-dimensional voltage angle vector with at least one non-zero element. For $K = 2$ it is easily verified that

$$\frac{\mathbf{1}}{\mathbf{2}}\delta(\mathbf{2})^{\mathbf{T}}\mathbf{W}(\mathbf{2})\delta(\mathbf{2}) \;=\; \pi\left[\delta_1 - \delta_2\right]^2 \;=\; \pi\left[\sum_{km \in BR} [\delta_k - \delta_m]^2\right] \;>\; 0 \tag{45}$$

Consequently, $\mathbf{W}(\mathbf{2})$ is a symmetric positive definite matrix. A simple induction argument on K then establishes that $\mathbf{W}(\mathbf{K})$ is a symmetric positive definite matrix for arbitrary $K \geq 2$.

Now suppose $\delta_1 \equiv 0$ and $\delta_k \neq 0$ for some $k = 2, \dots, K$, and let $\delta_{-1}^T(K) = [\delta_2 \dots \delta_K]$. Also, let $\mathbf{W_{rr}}(\mathbf{K})$ denote the *reduced weight matrix* constructed from $\mathbf{W}(\mathbf{K})$ by deleting its first row and its first column as follows:

$$\mathbf{W_{rr}}(\mathbf{K}) = 2\pi \begin{bmatrix} \sum_{k \neq 2} \mathbb{E}_{k2} & -\mathbb{E}_{23} & \cdots & -\mathbb{E}_{2K} \\ -\mathbb{E}_{32} & \sum_{k \neq 3} \mathbb{E}_{k3} & \cdots & -\mathbb{E}_{3K} \\ \vdots & \vdots & \ddots & \vdots \\ -\mathbb{E}_{K2} & -\mathbb{E}_{K3} & \cdots & \sum_{k \neq K} \mathbb{E}_{kK} \end{bmatrix}_{(K-1)\times(K-1)} \tag{46}$$

It is then easily shown by a simple induction argument that

$$\begin{aligned} \frac{\mathbf{1}}{\mathbf{2}}\delta(\mathbf{K})^{\mathbf{T}}\mathbf{W}(\mathbf{K})\delta(\mathbf{K}) \;&=\; \frac{\mathbf{1}}{\mathbf{2}}\delta_{\mathbf{-1}}(\mathbf{K})^{\mathbf{T}}\mathbf{W_{rr}}(\mathbf{K})\delta_{\mathbf{-1}}(\mathbf{K}) \\ &=\; \pi\left[\sum_{1m \in BR} \delta_m^2 \;+\; \sum_{km \in BR,\; k \geq 2} [\delta_k - \delta_m]^2\right] \;>\; 0 \end{aligned} \tag{47}$$

Consequently, $\mathbf{W_{rr}}(\mathbf{K})$ is a symmetric positive definite matrix whose quadratic form expresses the soft penalty term in the augmented DC OPF objective function (35). For expositional simplicity, the dimension argument K for this matrix will hereafter be suppressed.

Let the Generators' *cost attribute matrix* $\mathbf{U}$ be defined as

$$\mathbf{U} = \mathrm{diag}[\,2B_1, 2B_2, \cdots, 2B_I] = \begin{bmatrix} 2B_1 & 0 & \cdots & 0 \\ 0 & 2B_2 & \cdots & 0 \\ \vdots & \vdots & \ddots & \vdots \\ 0 & 0 & \cdots & 2B_I \end{bmatrix}_{I \times I} \tag{48}$$

Recalling from Table 1 that the Generator cost coefficients B_i are assumed to be strictly positive, it is easily seen that $\mathbf{U}$ is a symmetric positive definite matrix.

Finally, let the matrix $\mathbf{G}$ be defined by

$$\mathbf{G} = \text{blockDiag}\left[\begin{array}{cc} \mathbf{U} & \mathbf{W_{rr}} \end{array}\right] = \left[\begin{array}{cc} \mathbf{U} & \mathbf{0} \\ \mathbf{0} & \mathbf{W_{rr}} \end{array}\right]_{(I+K-1)\times(I+K-1)} \tag{49}$$

The matrix $\mathbf{G}$ is clearly symmetric. Moreover, $\mathbf{G}$ is positive definite since its associated quadratic form maps any vector $\mathbf{x^T} = [P_{G1}, \ldots, P_{GI}, \delta_2, \ldots, \delta_K]$ with at least one non-zero component into a strictly positive scalar. That is,

$$\frac{\mathbf{1}}{\mathbf{2}}\mathbf{x^T G x} \;=\; \sum_{i=1}^{I}[B_i P_{Gi}^2] \;+\; \pi\left[\sum_{1m\in BR}\delta_m^2 + \sum_{km\in BR,\ k\geq 2}[\delta_k - \delta_m]^2\right] \;>\; 0 \tag{50}$$

In particular, comparing (50) with (35), it is seen that (50) provides a positive definite quadratic form representation for the nonlinear terms in the augmented DC OPF objective function.

4.2 Constraint Depiction

The main factor complicating the matrix representation of the constraints for the augmented DC OPF problem is, once again, the need to allow for the possible absence of direct branch connections between nodes. This subsection derives special matrices to facilitate this constraint representation.

Let the definition (17) for B_{km} be extended for all $k \neq m$ as follows:

$$B_{km} \;=\; \begin{cases} \frac{1}{x_{km}\ \text{pu}} \;>\; 0 & \text{if } km \text{ or } mk \in BR \\ \\ 0 & \text{otherwise} \end{cases}$$

Since x_{km} pu $= x_{mk}$ pu for all $km \in BR$, it follows that $B_{km} = B_{mk}$ for all $k \neq m$. Using this definition for B_{km}, construct the *bus admittance matrix* $\mathbf{B'}$ as follows:

$$\mathbf{B'} = \left[\begin{array}{ccccc} \sum_{k\neq 1} B_{k1} & -B_{12} & -B_{13} & \cdots & -B_{1K} \\ -B_{21} & \sum_{k\neq 2} B_{k2} & -B_{23} & \cdots & -B_{2K} \\ -B_{31} & -B_{32} & \sum_{k\neq 3} B_{k3} & \cdots & -B_{3K} \\ \vdots & \vdots & \vdots & \ddots & \vdots \\ -B_{K1} & -B_{K2} & -B_{K3} & \cdots & \sum_{k\neq K} B_{kK} \end{array}\right]_{K\times K} \tag{51}$$

The *reduced bus admittance matrix* $\mathbf{B'_r}$ consisting of $\mathbf{B'}$ with its first row omitted then takes the following form:

$$\mathbf{B}'_{\mathbf{r}} = \begin{bmatrix} -B_{21} & \sum_{k\neq 2} B_{k2} & -B_{23} & \cdots & -B_{2K} \\ -B_{31} & -B_{32} & \sum_{k\neq 3} B_{k3} & \cdots & -B_{3K} \\ \vdots & \vdots & \vdots & \ddots & \vdots \\ -B_{K1} & -B_{K2} & -B_{K3} & \cdots & \sum_{k\neq K} B_{kK} \end{bmatrix}_{(K-1)\times K} \tag{52}$$

Let **BI** denote the listing of the N distinct branches $km \in BR$ constituting the transmission grid, lexicographically sorted as in a dictionary from lower to higher numbered nodes. Let $\mathbf{BI}_n$ denote the nth branch listed in **BI**. Then the *adjacency matrix* $\mathbb{A}$ with entries of 1 for the "from" node and -1 for the "to" node can be expressed as follows:

$$\mathbb{A} = \begin{bmatrix} \mathbb{J}(1,\mathbf{BI}_1) & \mathbb{J}(2,\mathbf{BI}_1) & \cdots & \mathbb{J}(K,\mathbf{BI}_1) \\ \mathbb{J}(1,\mathbf{BI}_2) & \mathbb{J}(2,\mathbf{BI}_2) & \cdots & \mathbb{J}(K,\mathbf{BI}_2) \\ \vdots & \vdots & \ddots & \vdots \\ \mathbb{J}(1,\mathbf{BI}_N) & \mathbb{J}(2,\mathbf{BI}_N) & \cdots & \mathbb{J}(K,\mathbf{BI}_N) \end{bmatrix}_{N\times K} \tag{53}$$

where $\mathbb{J}(\cdot)$ is an indicator function defined as:

$$\mathbb{J}(i,\mathbf{BI}_n) = \begin{cases} +1 & \text{if } \mathbf{BI}_n \text{ takes the form } ij \in BR \text{ for some node } j > i \\ -1 & \text{if } \mathbf{BI}_n \text{ takes the form } ji \in BR \text{ for some node } j < i \\ 0 & \text{otherwise} \end{cases}$$

$$\text{for all nodes } i = 1, ..., K \text{ and for all branches } n = 1, ..., N$$

Let the *reduced adjacency matrix* $\mathbb{A}_{\mathbf{r}}$ be defined as $\mathbb{A}$ with its first column deleted. Thus, $\mathbb{A}_{\mathbf{r}}$ is expressed as

$$\mathbb{A}_{\mathbf{r}} = \begin{bmatrix} \mathbb{J}(2,\mathbf{BI}_1) & \cdots & \mathbb{J}(K,\mathbf{BI}_1) \\ \mathbb{J}(2,\mathbf{BI}_2) & \cdots & \mathbb{J}(K,\mathbf{BI}_2) \\ \vdots & \ddots & \vdots \\ \mathbb{J}(2,\mathbf{BI}_N) & \cdots & \mathbb{J}(K,\mathbf{BI}_N) \end{bmatrix}_{N\times(K-1)} \tag{54}$$

Also, define the matrix **II** by

$$\mathbf{II} = \begin{bmatrix} \mathbb{I}(1 \in I_1) & \mathbb{I}(2 \in I_1) & \cdots & \mathbb{I}(I \in I_1) \\ \mathbb{I}(1 \in I_2) & \mathbb{I}(2 \in I_2) & \cdots & \mathbb{I}(I \in I_2) \\ \vdots & \vdots & \ddots & \vdots \\ \mathbb{I}(1 \in I_K) & \mathbb{I}(2 \in I_K) & \cdots & \mathbb{I}(I \in I_K) \end{bmatrix}_{K\times I} \tag{55}$$

where

$$\mathbb{I}(i \in I_k) = \begin{cases} 1 & \text{if } i \in I_k \\ 0 & \text{if } i \notin I_k \end{cases}$$

for each $i = 1, \ldots, I$ and $k = 1, \ldots, K$. Finally, define the matrix $\mathbf{D}$ to be the diagonal matrix whose diagonal entries give the B_{km} values for all distinct connected branches $km \in BR$ ordered as in BI. That is, with some slight abuse of notation:

$$\mathbf{D} = \text{diag}\left[\begin{array}{cccc} D_1 & D_2 & \cdots & D_N \end{array}\right]_{N\times N} \tag{56}$$

where $D_n = B_{km}$ if BI_n (the nth element of BI) corresponds to branch $km \in BR$.[15]

4.3 The Complete SCQP Depiction

Using the notation from Sections 4.1 and 4.2, the complete SCQP depiction for the augmented DC OPF problem in reduced pu form set out in Section 3.4 can be expressed as follows:

Minimize

$$\mathbf{f(x)} = \frac{\mathbf{1}}{\mathbf{2}}\mathbf{x^T G x} + \mathbf{a^T x} \tag{57}$$

with respect to

$$\mathbf{x} = \left[\begin{array}{ccccccc} P_{G1} & \ldots & P_{GI} & \delta_2 & \ldots & \delta_K \end{array}\right]^{\mathbf{T}}_{(I+K-1)\times 1}$$

subject to

$$\mathbf{C_{eq}^T x} = \mathbf{b_{eq}} \tag{58}$$

$$\mathbf{C_{iq}^T x} \geq \mathbf{b_{iq}} \tag{59}$$

In this SCQP depiction, the symmetric positive definite matrix $\mathbf{G}$ is defined as in (49), and the vector $\mathbf{a^T}$ is given by

$$\mathbf{a}^T = \left[\begin{array}{cccccc} A_1 & \cdots & A_I & 0 & \cdots & 0 \end{array}\right]_{1\times(I+K-1)}$$

The equality constraint matrix $\mathbf{C_{eq}^T}$ takes the form:

$$\mathbf{C_{eq}^T} = \left[\begin{array}{cc} \mathbf{II} & -\mathbf{B_r'^T} \end{array}\right]_{K\times(I+K-1)}$$

where $\mathbf{B_r'}$ is defined as in (52) and $\mathbf{II}$ is defined as in (55). The associated equality constraint vector $\mathbf{b_{eq}}$ takes the form:

$$\mathbf{b_{eq}} = \left[\begin{array}{cccc} \sum_{j\in J_1} P_{Lj} & \sum_{j\in J_2} P_{Lj} & \cdots & \sum_{j\in J_K} P_{Lj} \end{array}\right]^{\mathbf{T}}_{K\times 1}$$

Finally, consider the inequality constraint matrix $\mathbf{C_{iq}}$. This matrix can be decomposed into several column-wise submatrices corresponding to the thermal constraints (37) (call it $\mathbf{C_{t1}}$), the thermal constraints (38) (call it $\mathbf{C_{t2}}$), the lower production constraints (39)

[15]Note that the matrix $\mathbf{H} \equiv \mathbf{D}\mathbb{A}_\mathbf{r}$ maps the vector $\delta = (\delta_2, \ldots, \delta_K)^T$ of voltage angles into the $N \times 1$ real power branch flow vector $\mathbf{F} \equiv \mathbf{H}\delta$. Also, as established in Appendix B, $\mathbf{PInject} = \mathbf{B'_{rr}}\delta$, where **PInject** denotes the $(K-1)\times 1$ vector of net nodal real power injections PNetInject_k, $k = 2, \ldots, K$, and $\mathbf{B'_{rr}}$ denotes the matrix $\mathbf{B'}$ in (51) with its first row and first column eliminated (corresponding to the reference node 1). Defining the *shift matrix* $\mathbf{S} \equiv \mathbf{H}[\mathbf{B'_{rr}}]^{-1}$, it follows that $\mathbf{F} = \mathbf{S}\cdot\mathbf{PInject}$. Compare CAISO (2003, pp. 24-25).

(call it $\mathbf{C_{pL}}$), and the upper production constraints (40) (call it $\mathbf{C_{pU}}$). Note, further, that $\mathbf{C_{t1}} = -\mathbf{C_{t2}}$ and $\mathbf{C_{pL}} = -\mathbf{C_{pU}}$. For easier notation, let $\mathbf{C_t} \equiv \mathbf{C_{t1}}$ and $\mathbf{C_p} \equiv \mathbf{C_{pL}}$. The inequality constraint constraint matrix $\mathbf{C_{iq}}$ can then be expressed as follows:

$$\mathbf{C_{iq}} = \left[\begin{array}{cccc} \mathbf{C_t} & -\mathbf{C_t} & \mathbf{C_p} & -\mathbf{C_p} \end{array} \right]_{(I+K-1)\times(2N+2I)}$$

or

$$\mathbf{C_{iq}^T} = \left[\begin{array}{cccc} \mathbf{C_t^T} & -\mathbf{C_t^T} & \mathbf{C_p^T} & -\mathbf{C_p^T} \end{array} \right]^{\mathbf{T}}_{(2N+2I)\times(I+K-1)}$$

In this expression,

$$\mathbf{C_t^T} = \left[\begin{array}{cc} \mathbf{O_t} & -\mathbf{D}\mathbb{A}_\mathbf{r} \end{array} \right]_{N\times(I+K-1)}$$

where $\mathbf{O_t}$ is an $N \times I$ zero matrix, $\mathbb{A}_\mathbf{r}$ is defined as in (54), and $\mathbf{D}$ is defined as in (56). Also,

$$\mathbf{C_p^T} = \left[\begin{array}{cc} \mathbf{I_p} & \mathbf{O_p} \end{array} \right]_{I\times(I+K-1)}$$

where $\mathbf{I_p}$ is an $I \times I$ identity matrix and $\mathbf{O_p}$ is an $I \times (K-1)$ zero matrix. Putting all these terms together, one has:

$$\mathbf{C_{iq}^T} = \left[\begin{array}{cc} \mathbf{O_t} & -\mathbf{D}\mathbb{A}_\mathbf{r} \\ -\mathbf{O_t} & \mathbf{D}\mathbb{A}_\mathbf{r} \\ \mathbf{I_p} & \mathbf{O_p} \\ -\mathbf{I_p} & -\mathbf{O_p} \end{array} \right]_{(2N+2I)\times(I+K-1)}$$

Finally, the associated inequality constraint vector $\mathbf{b_{iq}}$ can be similarly decomposed as follows:

$$\mathbf{b_{iq}} = \left[\begin{array}{cccc} \mathbf{b_t} & \mathbf{b_t} & \mathbf{b_{pL}} & \mathbf{b_{pU}} \end{array} \right]^{\mathbf{T}}_{(2N+2I)\times 1}$$

where

$$\mathbf{b_t} = \left[\begin{array}{cccc} -F^U_{\mathbf{BI}_1} & -F^U_{\mathbf{BI}_2} & \cdots & -F^U_{\mathbf{BI}_N} \end{array} \right]^{\mathbf{T}}_{N\times 1}$$

$$\mathbf{b_{pL}} = \left[\begin{array}{cccc} P^L_{G1} & P^L_{G2} & \cdots & P^L_{GI} \end{array} \right]^{\mathbf{T}}_{I\times 1}$$

$$\mathbf{b_{pU}} = \left[\begin{array}{cccc} -P^U_{G1} & -P^U_{G2} & \cdots & -P^U_{GI} \end{array} \right]^{\mathbf{T}}_{I\times 1}$$

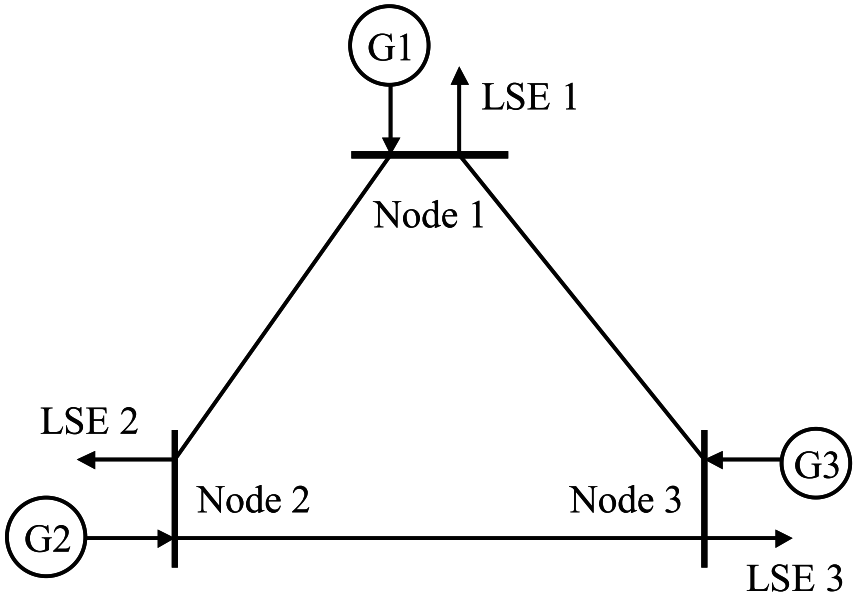

Figure 1: A Three-Node Transmission Grid

5 Illustrative Examples

5.1 A Three-Node Illustration

Consider the special case of a completely connected transmission grid consisting of three nodes $\{1, 2, 3\}$, three Generators, and three LSEs, with Generator k and LSE k located at node k for $k = 1, 2, 3$. This three-node case is depicted in Figure 1.

For this three-node case, the augmented DC OPF problem set out in Section 3.4 reduces to the following form:

Minimize

$$\sum_{i=1}^{3}[A_i P_{Gi} + B_i P_{Gi}^2] + \pi\delta_2^2 + \pi\delta_3^2 + \pi[\delta_2 - \delta_3]^2 \tag{60}$$

with respect to

$$P_{G1}, P_{G2}, P_{G3}, \delta_2, \delta_3$$

subject to:

Real power balance constraint for each node k = 1, ..., 3:

$$P_{G1} + B_{12}\delta_2 + B_{13}\delta_3 = P_{L1} \tag{61}$$

$$P_{G2} - [B_{12} + B_{23}]\delta_2 + B_{23}\delta_3 = P_{L2} \tag{62}$$

$$P_{G3} + B_{23}\delta_2 - [B_{13} + B_{23}]\delta_3 = P_{L3} \tag{63}$$

Real power thermal constraints for each branch km $\in$ BR:

$$B_{12}\delta_2 \geq -F_{12}^U \tag{64}$$

$$B_{13}\delta_3 \geq -F_{13}^U \tag{65}$$

$$-B_{23}\delta_2 + B_{23}\delta_3 \geq -F_{23}^U \tag{66}$$

$$-B_{12}\delta_2 \geq -F_{12}^U \tag{67}$$

$$-B_{13}\delta_3 \geq -F_{13}^U \tag{68}$$

$$B_{23}\delta_2 - B_{23}\delta_3 \geq -F_{23}^U \tag{69}$$

Real power production constraints for each Generator i $= 1, ..., 3$:

$$P_{G1} \geq P_{G1}^L \tag{70}$$

$$P_{G2} \geq P_{G2}^L \tag{71}$$

$$P_{G3} \geq P_{G3}^L \tag{72}$$

$$-P_{G1} \geq -P_{G1}^U \tag{73}$$

$$-P_{G2} \geq -P_{G2}^U \tag{74}$$

$$-P_{G3} \geq -P_{G3}^U \tag{75}$$

Using the notation introduced in Section 4, the SCQP depiction for this three-node case is as follows:

Minimize

$$\mathbf{f(x)} = \frac{\mathbf{1}}{\mathbf{2}}\mathbf{x^T G x} + \mathbf{a^T x} \tag{76}$$

with respect to

$$\mathbf{x} \;=\; [P_{G1}, P_{G2}, P_{G3}, \delta_2, \delta_3]^{\mathbf{T}}_{(5\times 1)} \tag{77}$$

subject to

$$\mathbf{C_{eq}^T x = b_{eq}} \tag{78}$$

$$\mathbf{C_{iq}^T x \geq b_{iq}} \tag{79}$$

where

$$\mathbf{G} = \begin{bmatrix} 2B_1 & 0 & 0 & 0 & 0 \\ 0 & 2B_2 & 0 & 0 & 0 \\ 0 & 0 & 2B_3 & 0 & 0 \\ 0 & 0 & 0 & 4\pi & -2\pi \\ 0 & 0 & 0 & -2\pi & 4\pi \end{bmatrix}_{(5\times5)}$$

$$\mathbf{a^T} = \begin{bmatrix} A_1 & A_2 & A_3 & 0 & 0 \end{bmatrix}_{(1\times5)}$$

$$\mathbf{C_{eq}^T} = \begin{bmatrix} 1 & 0 & 0 & B_{12} & B_{13} \\ 0 & 1 & 0 & -[B_{12}+B_{23}] & B_{23} \\ 0 & 0 & 1 & B_{23} & -[B_{13}+B_{23}] \end{bmatrix}_{(3\times5)}$$

$$\mathbf{b_{eq}} = \begin{bmatrix} P_{L1} & P_{L2} & P_{L3} \end{bmatrix}^{\mathbf{T}}_{(3\times1)}$$

$$\mathbf{C_{iq}^T} = \begin{bmatrix} 0 & 0 & 0 & B_{12} & 0 \\ 0 & 0 & 0 & 0 & B_{13} \\ 0 & 0 & 0 & -B_{23} & B_{23} \\ 0 & 0 & 0 & -B_{12} & 0 \\ 0 & 0 & 0 & 0 & -B_{13} \\ 0 & 0 & 0 & B_{23} & -B_{23} \\ 1 & 0 & 0 & 0 & 0 \\ 0 & 1 & 0 & 0 & 0 \\ 0 & 0 & 1 & 0 & 0 \\ -1 & 0 & 0 & 0 & 0 \\ 0 & -1 & 0 & 0 & 0 \\ 0 & 0 & -1 & 0 & 0 \end{bmatrix}_{(12\times5)}$$

$$\mathbf{b_{iq}} = \begin{bmatrix} -F_{12}^U & -F_{13}^U & -F_{23}^U & -F_{12}^U & -F_{13}^U & -F_{23}^U & P_{G1}^L & P_{G2}^L & P_{G3}^L & -P_{G1}^U & -P_{G2}^U & -P_{G3}^U \end{bmatrix}^{\mathbf{T}}_{(12\times1)}$$

Note that the first six rows in matrix $\mathbf{C_{iq}^T}$ correspond to thermal inequality constraints and the next six rows correspond to power production inequality constraints.

5.2 A Five-Node Illustration

Now consider a five-node case for which the transmission grid is not completely connected. As depicted in Figure 2, let five Generators and three LSEs be distributed across the grid as follows: Generators 1 and 2 are located at node 1; LSE 1 is located at node 2; Generator 3 and LSE 2 are located at node 3; Generator 4 and LSE 3 are located at node 4; and Generator 5 is located node 5.

This information implies the following structural configuration for the transmission grid:

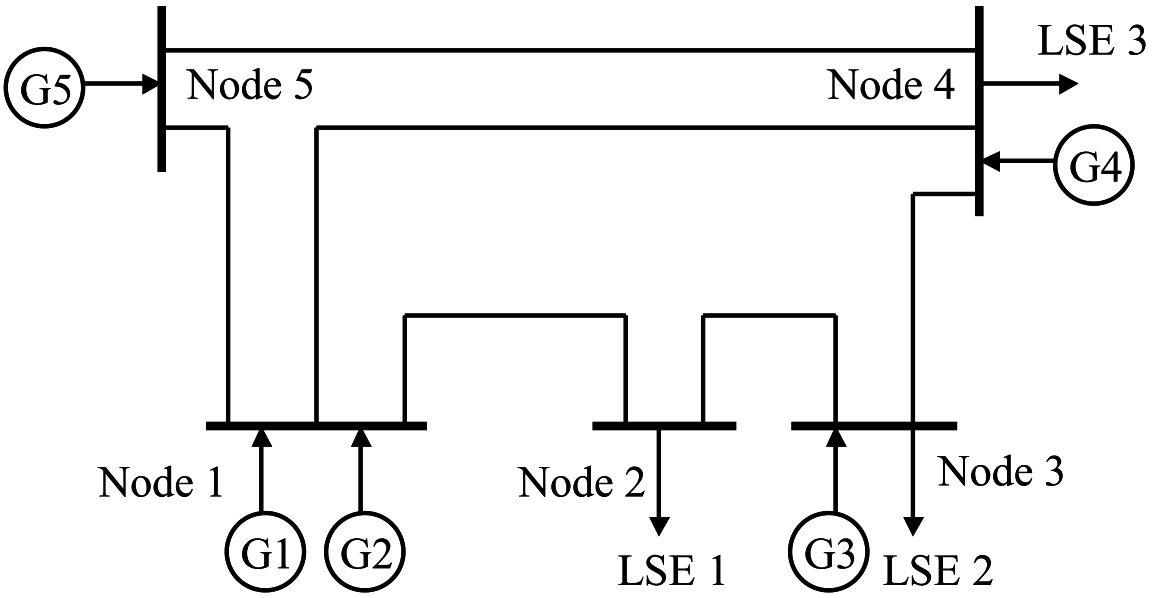

Figure 2: A Five-Node Transmission Grid

$$K = 5;\ I = 5;\ J = 3;$$

$$I_1 = \{\text{G1}, \text{G2}\},\ I_2 = \{\emptyset\},\ I_3 = \{\text{G3}\},\ I_4 = \{\text{G4}\},\ I_5 = \{\text{G5}\};$$

$$J_1 = \{\emptyset\},\ J_2 = \{\text{LSE1}\},\ J_3 = \{\text{LSE2}\},\ J_4 = \{\text{LSE3}\},\ J_5 = \{\emptyset\};$$

$$\sum_{j\in J_1} P_{Lj} = 0,\ \sum_{j\in J_2} P_{Lj} = P_{L_1},\ \sum_{j\in J_3} P_{Lj} = P_{L_2},\ \sum_{j\in J_4} P_{Lj} = P_{L_3},\ \sum_{j\in J_5} P_{Lj} = 0;$$

The distinct directly-connected node pairs are (1,2), (1,4), (1,5), (2,3), (3,4), (4,5), which implies that the number of distinct transmission grid branches is $N = 6$. The branch connection matrix $\mathbb{E}$ can be written as follows:

$$\mathbb{E} = \begin{bmatrix} 0 & 1 & 0 & 1 & 1 \\ 1 & 0 & 1 & 0 & 0 \\ 0 & 1 & 0 & 1 & 0 \\ 1 & 0 & 1 & 0 & 1 \\ 1 & 0 & 0 & 1 & 0 \end{bmatrix}_{5\times 5} \tag{80}$$

The weight matrix $\mathbf{W}$ and its reduced form $\mathbf{W_{rr}}$ are

$$\mathbf{W} = 2\pi \begin{bmatrix} 3 & -1 & 0 & -1 & -1 \\ -1 & 2 & -1 & 0 & 0 \\ 0 & -1 & 2 & -1 & 0 \\ -1 & 0 & -1 & 3 & -1 \\ -1 & 0 & 0 & -1 & 2 \end{bmatrix}_{5\times 5} \tag{81}$$

$$\mathbf{W_{rr}} = 2\pi \begin{bmatrix} 2 & -1 & 0 & 0 \\ 1 & 2 & -1 & 0 \\ 0 & -1 & 3 & -1 \\ 0 & 0 & -1 & 2 \end{bmatrix}_{4\times 4} \tag{82}$$

The Generators' cost attribute matrix $\mathbf{U}$ is:

$$\mathbf{U} = \text{diag}\begin{bmatrix} 2B_1 & 2B_2 & 2B_3 & 2B_4 & 2B_5 \end{bmatrix}_{5\times 5} \tag{83}$$

The matrix $\mathbf{B'}$ and its reduced form $\mathbf{B'_r}$ are as follows:

$$\mathbf{B'} = \begin{bmatrix} B_{12}+B_{14}+B_{15} & -B_{12} & 0 & -B_{14} & -B_{15} \\ -B_{21} & B_{21}+B_{23} & -B_{23} & 0 & 0 \\ 0 & -B_{32} & B_{32}+B_{34} & -B_{34} & 0 \\ -B_{41} & 0 & -B_{43} & B_{41}+B_{43}+B_{45} & -B_{45} \\ -B_{51} & 0 & 0 & -B_{54} & B_{51}+B_{54} \end{bmatrix}_{5\times 5} \tag{84}$$

$$\mathbf{B'_r} = \begin{bmatrix} -B_{21} & B_{21}+B_{23} & -B_{23} & 0 & 0 \\ 0 & -B_{32} & B_{32}+B_{34} & -B_{34} & 0 \\ -B_{41} & 0 & -B_{43} & B_{41}+B_{43}+y_{45} & -B_{45} \\ -B_{51} & 0 & 0 & -B_{54} & B_{51}+B_{54} \end{bmatrix}_{4\times 5} \tag{85}$$

With a slight abuse of notation, the ordered list $\mathbf{BI}$ of distinct transmission grid branches can be denoted as follows:

$$\mathbf{BI} = [(1,2),(1,4),(1,5),(2,3),(3,4),(4,5)]^T_{6\times 1} \tag{86}$$

The adjacency matrix $\mathbb{A}$ with entries of 1 for the "from" node and -1 for the "to" node can be expressed as

$$\mathbb{A} = \begin{bmatrix} 1 & -1 & 0 & 0 & 0 \\ 1 & 0 & 0 & -1 & 0 \\ 1 & 0 & 0 & 0 & -1 \\ 0 & 1 & -1 & 0 & 0 \\ 0 & 0 & 1 & -1 & 0 \\ 0 & 0 & 0 & 1 & -1 \end{bmatrix}_{6\times 5} \tag{87}$$

and its reduced form $\mathbb{A}_\mathbf{r}$ can be expressed as

$$\mathbb{A}_\mathbf{r} = \begin{bmatrix} -1 & 0 & 0 & 0 \\ 0 & 0 & -1 & 0 \\ 0 & 0 & 0 & -1 \\ 1 & -1 & 0 & 0 \\ 0 & 1 & -1 & 0 \\ 0 & 0 & 1 & -1 \end{bmatrix}_{6\times 4} \tag{88}$$

The matrix **II** takes the form

$$\mathbf{II} = \begin{bmatrix} 1 & 1 & 0 & 0 & 0 \\ 0 & 0 & 0 & 0 & 0 \\ 0 & 0 & 1 & 0 & 0 \\ 0 & 0 & 0 & 1 & 0 \\ 0 & 0 & 0 & 0 & 1 \end{bmatrix}_{5\times 5} \tag{89}$$

Finally, the matrix **D** takes the form

$$\mathbf{D} = \text{diag}\begin{bmatrix} B_{12} & B_{14} & B_{15} & B_{23} & B_{34} & B_{45} \end{bmatrix}_{6\times 6} \tag{90}$$

Using the above developments, the SCQP depiction for the augmented DC-OPF problem for this five-node case can be expressed as follows:

Minimize

$$\mathbf{f(x)} = \frac{\mathbf{1}}{\mathbf{2}}\mathbf{x^T G x} + \mathbf{a^T x}$$

with respect to

$$\mathbf{x} = \begin{bmatrix} P_{G1} & P_{G2} & P_{G3} & P_{G4} & P_{G5} & \delta_2 & \delta_3 & \delta_4 & \delta_5 \end{bmatrix}^{\mathbf{T}}_{9\times 1}$$

subject to

$$\mathbf{C_{eq}^T x} = \mathbf{b_{eq}}$$

$$\mathbf{C_{iq}^T x} \geq \mathbf{b_{iq}}$$

where the input matrices and vectors $\mathbf{G}$, $\mathbf{a^T}$, $\mathbf{C_{eq}^T}$, $\mathbf{b_{eq}}$, $\mathbf{C_{iq}^T}$, and $\mathbf{b_{iq}}$ take the following explicit forms:

$$\mathbf{G} = \text{blockDiag}\begin{bmatrix} \mathbf{U} & \mathbf{W_{rr}} \end{bmatrix}_{9\times 9}$$

$$\mathbf{a^T} = \begin{bmatrix} A_1 & A_2 & A_3 & A_4 & A_5 & 0 & 0 & 0 & 0 \end{bmatrix}_{1\times 9}$$

$$\mathbf{C_{eq}^T} = \begin{bmatrix} \mathbf{II} & -\mathbf{B_r'^T} \end{bmatrix}_{5\times 9}$$

where

$\mathbf{B_r'}$ is defined as in (85)

II is defined as in (89)

$$\mathbf{b_{eq}} = \begin{bmatrix} 0 & P_{L1} & P_{L2} & P_{L3} & 0 \end{bmatrix}^{\mathbf{T}}_{5\times 1}$$

$$\mathbf{C_{iq}^T} = \left[\begin{array}{cccc} \mathbf{C_t^T} & -\mathbf{C_t^T} & \mathbf{C_p^T} & -\mathbf{C_p^T} \end{array} \right]_{22\times 9}^{\mathbf{T}}$$

where

$$\mathbf{C_t^T} = \left[\begin{array}{cc} \mathbf{O_t} & -\mathbf{D}\mathbb{A}_\mathbf{r} \end{array} \right]_{6\times 9}$$

$\mathbf{O_t} = 6 \times 5$ zero matrix

$\mathbb{A}_\mathbf{r}$ is defined as in (88)

$\mathbf{D}$ is defined as in (90)

$$\mathbf{C_p^T} = \left[\begin{array}{cc} \mathbf{I_p} & \mathbf{O_p} \end{array} \right]_{5\times 9}$$

$\mathbf{I_p} = 5 \times 5$ identity matrix

$\mathbf{O_p} = 5 \times 4$ zero matrix

$$\mathbf{b_{iq}} = \left[\begin{array}{cccc} \mathbf{b_t} & \mathbf{b_t} & \mathbf{b_{pL}} & \mathbf{b_{pU}} \end{array} \right]_{22\times 1}^{\mathbf{T}}$$

where

$$\mathbf{b_t} = \left[\begin{array}{cccccc} -F_{12}^U & -F_{14}^U & -F_{15}^U & -F_{23}^U & -F_{34}^U & -F_{45}^U \end{array} \right]_{6\times 1}^{\mathbf{T}}$$

$$\mathbf{b_{pL}} = \left[\begin{array}{ccccc} P_{G1}^L & P_{G2}^L & P_{G3}^L & P_{G4}^L & P_{G5}^L \end{array} \right]_{5\times 1}^{\mathbf{T}}$$

$$\mathbf{b_{pU}} = \left[\begin{array}{ccccc} -P_{G1}^U & -P_{G2}^U & -P_{G3}^U & -P_{G4}^U & -P_{G5}^U \end{array} \right]_{5\times 1}^{\mathbf{T}}$$

6 QuadProgJ Input/Output and Logical Progression

The matrix form of a general SCQP problem is presented in Section 1. QuadProgJ accepts input in this matrix form. In particular, QuadProgJ can be directly used to solve any DC OPF problem expressed in this matrix form whether the DC OPF variables are expressed in standard SI units (e.g. ohms, megawatts,...) or in normalized per unit (pu) terms.

On the other hand, to help ensure numerical stability, it is customary when solving DC OPF problems to carry out all internal calculations in pu terms so that variables have roughly the same order of magnitude. The pu solution output is then often converted back into SI units for easier readability.

Consequently, to facilitate the application of QuadProgJ to DC OPF problems, we have developed an optional outer Java shell for QuadProgJ, referred to as *DCOPFJ*, that carries out the following data manipulations: (a) accepts DC OPF input data in SI units and

converts it to pu; (b) uses this pu input data to form the SCQP matrix and vector expressions required by QuadProgJ; (c) invokes QuadProgJ to solve this SCQP problem; (d) converts the resulting pu solution output back into SI units.

Consider the augmented DC OPF problem set out in Section 3.4. The required input data for this problem, expressed in SI units, can be schematically depicted as follows:

$$\text{(SI gridData, SI genData, SI lseData)}$$

where

$$\begin{aligned}
\text{SI gridData} &= \text{(SI nodeData, SI branchData)} \\
\text{SI nodeData} &= (K,\ \pi) \\
\text{SI branchData} &= (\mathbf{BI},\ p^U_{\mathbf{BI}_1}...p^U_{\mathbf{BI}_N}, X \text{ ohms}) \\
\text{SI genData} &= (I,\ I_1...I_K, a_1...a_I,\ b_1...b_I,\ p^L_{G1}...p^L_{GI},\ p^U_{G1}...p^U_{GI}) \\
\text{SI lseData} &= (J,\ J_1...J_K, \sum_{j\in J_1} p_{Lj}\ ...\ \sum_{j\in J_K} p_{Lj})
\end{aligned}$$

This SI input data is fed into DCOPFJ along with a base apparent power value S_o and a base voltage value V_o. The DCOPFJ shell first uses the base values to transform the SI input data into pu terms. Using the pu notation introduced in Section 3.1, this pu input data can be schematically depicted as follows:

$$\text{(pu gridData, pu genData, pu lseData)}$$

where

$$\begin{aligned}
\text{pu gridData} &= \text{(pu nodeData, pu branchData)} \\
\text{pu nodeData} &= (K,\ \pi) \\
\text{pu branchData} &= (\mathbf{BI},\ F^U_{\mathbf{BI}_1}...F^U_{\mathbf{BI}_N}, X \text{ pu}) \\
\text{pu genData} &= (I,\ I_1...I_K, A_1...A_I,\ B_1...B_I,\ P^L_{G1}...P^L_{GI},\ P^U_{G1}...P^U_{GI}) \\
\text{pu lseData} &= (J,\ J_1...J_K, \sum_{j\in J_1} P_{Lj}\ ...\ \sum_{j\in J_K} P_{Lj})
\end{aligned}$$

DCOPFJ next uses this pu input data to form the matrices and vectors $(\mathbf{G}, \mathbf{a}, \mathbf{C_{eq}}, \mathbf{b_{eq}}, \mathbf{C_{iq}}, \mathbf{b_{iq}})$ as detailed in Section 4.3. It then feeds these matrix and vector components into the QuadProgJ solver to obtain a solution in pu terms. This pu solution can be expressed in the following vector form:

$$(P^*_{G1}...P^*_{GI},\ \delta^*_2...\delta^*_K,\ \lambda^*_{eq},\ \lambda^*_{iq}) \tag{91}$$

In this output vector, $(P^*_{G1}...P^*_{GI})$ denotes the vector of optimal pu real power production commitments in the day-ahead market for Generators $i = 1, \ldots, I$, and $(\delta^*_2...\delta^*_K)$ denotes the vector of optimal voltage angles (in radians) at nodes $k = 2, \ldots, K$ (omitting the reference node 1 where δ_1 is normalized to 0). The solution vector for the Lagrange multipliers

corresponding to the equality constraints is contained in the $K \times 1$ vector λ^*_{eq}. Since each of these multipliers is a shadow price corresponding to a nodal balance constraint in pu form, λ^*_{eq} provides the vector of Locational Marginal Prices (LMPs) in pu form.

The solution vector for the Lagrange multipliers corresponding to the inequality constraints is contained in the $(2N + 2I) \times 1$ vector λ^*_{iq}. These multipliers provide valuable additional sensitivity information, including "flow gate" prices (in pu) measuring the optimal cost reductions that would result from relaxations in the branch flow constraints.

Finally, the pu solution (91) is fed back into DCOPFJ for conversion into SI units for reporting purposes. Recalling from Section 3.1 that pu real power terms are obtained from SI real power terms (in MWs) by dividing through by the base apparent power S_o, this SI output data can be schematically depicted as follows:

$$(p^*_{G1} ... p^*_{GI},\ \delta^*_2 ... \delta^*_K,\ \lambda^*_{eq}/S_o,\ \lambda^*_{iq}/S_o)\ , \tag{92}$$

where the voltage angles δ^*_k are still reported in radians.

In summary, the overall logical flow of the QuadProgJ program can be depicted as follows:

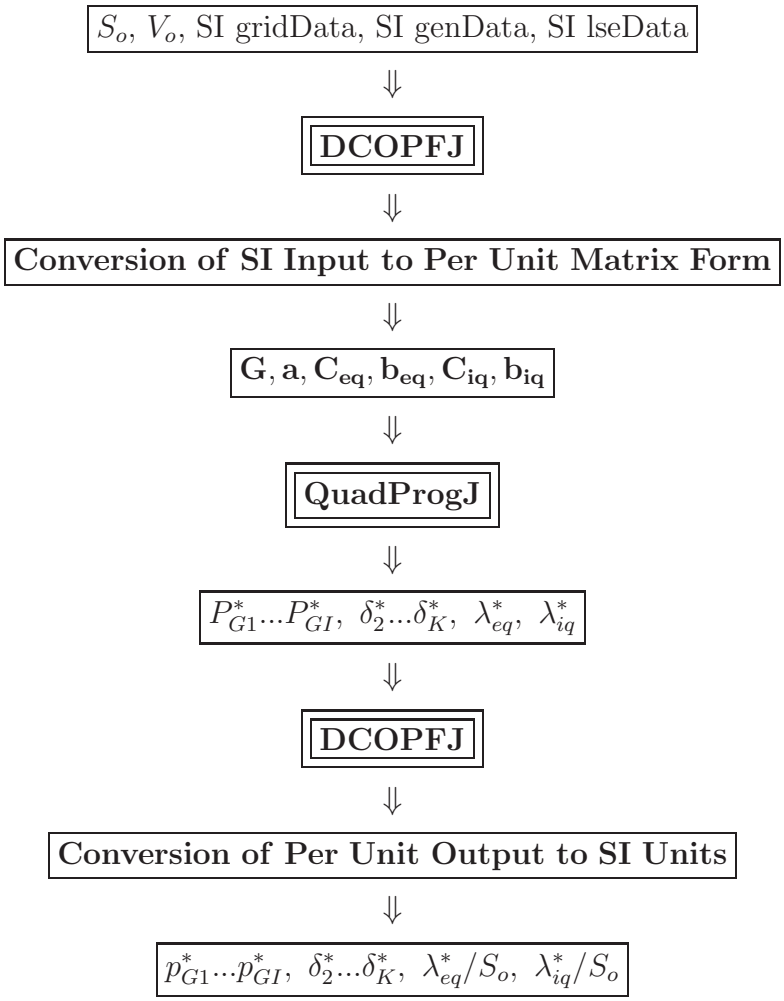

7 QP Test Results for QuadProgJ

7.1 Overview

QuadProgJ is a stand-alone open-source Java SCQP solver newly developed by the authors. QuadProgJ implements the well-known dual active-set SCQP method developed by Goldfarb and Idnani (1983) in a numerically stable way by utilizing Cholesky decomposition and QR factorization. For ease of use, QuadProgJ modifies the original Goldfarb and Idnani method to permit the direct explicit imposition of equality as well as inequality constraints.

As with any dual active-set SCQP method (Fletcher, 1987, pp. 243-245), QuadProgJ proceeds as follows. In the first iteration all problem constraints are ignored and the tentative optimal solution is taken to be the unconstrained minimum (which exists by strict convexity of the objective function). A test is then made to see if any of the original problem constraints are violated. If so, one of these violated constraints is selected and added to the "active set," i.e., the set of constraints to be imposed as equalities. A new optimal solution is then generated, subject to the active set of constraints, and again a test is made to see if any of the original problem constraints are violated. If so, one is selected to be added to the active set (and a test is made to see if any of the previously active constraints should now be relaxed). A new constrained optimal solution is then generated. This process continues until no violated original problem constraints are found.

Compared to other QP methods, such as interior point and primal active-set QP methods, a dual active-set SCQP method such as QuadProgJ has two major advantages. First, it has a well-defined starting point: namely, the unconstrained minimum of the objective function. In contrast, other types of methods typically have to guess or search for a "good" starting point, which can be very costly in terms of actual computing time. Second, since there are only finitely many distinct permutations of the inequality constraints to determine which if any are active (binding), and each activated constraint leads to an increase in the current objective function value, a dual active-set SCQP method is guaranteed to terminate in a finite number of steps. Infinite looping can arise with other types of methods for reasons such as a flat starting point.

On the downside, however, QuadProgJ has two main limitations. First, QuadProgJ requires the QP objective function to be a strictly convex function.[16] Second, QuadProgJ does not incorporate sparse matrix techniques. Consequently, it is not designed to handle large-scale problems for which speed and efficiency of computations become critical limiting factors.

In this section a well-known repository of QP test cases is used to demonstrate the accuracy of QuadProgJ for small to medium-scale QP problems.

[16] See Section 3.3.2 for brief notes on Lagrangian augmentation methods that can be used to induce strict convexity for convex QP objective functions. Solution algorithms designed to handle non-strictly convex QP problems have been developed by Boland (1997), Fletcher (1987), Powell (1983), and Stoer (1992).

7.2 QP Test Case Results

The accuracy of QuadProgJ has been tested on a collection of small to medium-sized SCQP minimization problems included in the QP test case repository prepared by Maros and Meszaros (1997).[17] For each of these problems, the solution value for the minimized objective function obtained by QuadProgJ is compared against the corresponding solution value reported for BPMPD, a well-known proprietary C-language QP solver implementing an interior-point algorithm.[18]

The general structure of these SCQP test cases is given in Table 3, along with the reported BPMPD solution values. Corresponding test case results for QuadProgJ are then reported in Table 4.[19] Specifically, Table 4 reports the relative difference (RD) between the minimum objective function value $f^* = f(x^*)$ obtained by QuadProgJ and the minimum objective function value fBPMPD attained by BPMPD, where

$$\text{RD} \equiv \frac{f^* - f\text{BPMPD}}{|f\text{BPMPD}|} \tag{93}$$

To help ensure a fair comparison, f^* has been rounded off to the same number of decimal places as fBPMPD.

In addition, Table 4 reports tests conducted to check whether all equality and inequality constraints are satisfied at the minimizing solution x^* obtained by QuadProgJ. More precisely, for any given SCQP test case, the equality constraints take the form

$$\mathbf{C_{eq}^T x} = \mathbf{b_{eq}} \tag{94}$$

and the inequality constraints take the form

$$\mathbf{C_{iq}^T x} \geq \mathbf{b_{iq}} \tag{95}$$

Let TNEC denote the total number of equality constraints for this test case (i.e. the row dimension of $\mathbf{C_{eq}^T}$), and let TNIC denote the total number of inequality constraints for this test case (i.e. the row dimension of $\mathbf{C_{iq}^T}$). Also, let x^* denote the solution obtained by QuadProgJ for this test case.

The equality constraints for each SCQP test case are checked by computing the *Equality Constraint Error (ECE)* for this test case, defined to be the TNEC $\times$ 1 residual vector

$$\text{ECE} \equiv \mathbf{C_{eq} x^*} - \mathbf{b_{eq}} \tag{96}$$

[17] Detailed input and output data for the SCQP test cases are available online at: http://www.sztaki.hu/~meszaros/public_ftp/qpdata/. Most of the test cases are in standard QPS format. The QPS format is an extension of the MPS format, which is the industrial standard format for linear programming test cases.

[18] See the BPMPD web site for detailed information. URL: http://www.sztaki.hu/~meszaros/bpmpd/

[19] All of the results reported in Table 4 for QuadProgJ were obtained from runs on a laptop PC: namely, a Compaq Presario 2100 running under Windows XP SP2 (mobile AMD Athlon XP 2800+ 2.12 GHz, 496 MB of RAM). The reported results for the BPMPD solver are taken from Maros and Meszaros (1997), who do not identify the hardware platform on which the BPMPD solver runs were made.

Table 3: SCQP Test Cases: Structural Attributes and BPMPD Solution Values

NAME[a]	TND[b]	TNEC[c]	TNIC[d]	TNC[e]	TN[f]	fBPMPD[g]
DUAL1	85	1	170	171	256	3.50129662E-02
DUAL2	96	1	192	193	289	3.37336761E-02
DUAL3	111	1	222	223	234	1.35755839E-01
DUAL4	75	1	150	151	226	7.46090842E-01
DUALC1	9	1	232	233	242	6.15525083E+03
DUALC5	8	1	293	294	302	4.27232327E+02
HS118	15	0	59	59	74	6.64820452E+02
HS21	2	0	5	5	7	-9.99599999E+01
HS268	5	0	5	5	10	5.73107049E-07
HS35	3	0	4	4	7	1.11111111E-01
HS35MOD	3	0	5	5	8	2.50000001E-01
HS76	4	0	7	7	11	-4.68181818E+00
KSIP	20	0	1001	1001	1021	5.757979412E-01
QPCBLEND	83	43	114	157	240	-7.84254092E-03
QPCBOEI1	384	9	971	980	1364	1.15039140E+07
QPCBOEI2	143	4	378	382	525	8.17196225E+06
QPCSTAIR	467	209	696	905	1372	6.20438748E+06
S268	5	0	5	5	10	5.73107049E-07
MOSARQP2	900	0	600	600	1500	-0.159748211E+04

[a]Case name (in QPS format), see Maros and Meszaros (1997) for a detailed description of the QPS format
[b]Total number of decision variables
[c]Total number of equality constraints
[d]Total number of inequality constraints
[e]Total number of constraints (equality and inequality). TNC=TNEC+TNIC
[f]Total number of decision variables and constraints (problem size). TN=TND+TNC
[g]Minimizing solution value obtained by the BPMPD solver on an unknown hardware platform

Table 4 reports the mean and maximum of the absolute values of the components of this ECE vector for each SCQP test case, denoted by Mean|ECE| and Max|ECE| respectively.

Similarly, the inequality constraints for each SCQP test case are checked by computing the *Inequality Constraint Error (ICE)*, defined to be the TNIC $\times$ 1 residual vector

$$\text{ICE} \quad \equiv \quad \mathbf{C_{iq}x^* - b_{iq}} \tag{97}$$

Table 4 reports the *Number of Violated Inequality Constraints (NVIC)* for each SCQP test case, meaning the number of negative components in this ICE vector.

Based on the results presented in Table 4, it appears that the QuadProgJ solver has an accuracy level slightly better than the BPMPD solver for small to medium-sized SCQP problems, that is, for SCQP problems for which the total number (TN) of decision variables plus constraints is less than 1500. This conclusion is supported by the observation that, for each of these test cases, the minimized objective function value $f^* = f(x^*)$ obtained by QuadProgJ either equals or is strictly smaller than the corresponding minimized objective

Table 4: QuadProgJ Test Case Results

NAME	Mean|ECE|[a]	Max|ECE|[b]	NVIC[c]	f*[d]	RD[e]
DUAL1	0.0	0.0	0	3.50129657E-2	-1.42804239E-8
DUAL2	0.0	0.0	0	3.37336761E-2	0.0
DUAL3	6.66E-16	6.66E-16	0	1.35755837E-1	-1.47323313E-8
DUAL4	2.11E-15	2.11E-15	0	7.46090842E-1	0.0
DUALC1	2.40E-12	2.40E-12	0	6.15525083E+3	0.0
DUALC5	5.33E-15	5.33E-15	0	4.27232327E+2	0.0
HS118	NA[f]	NA	0	6.64820450E+2	-3.00833103E-9
HS21	NA	NA	0	-99.96	-1.00040010E-9
HS268	NA	NA	0	-5.47370291E-8	-1.09550926
HS35	NA	NA	0	1.11111111E-1	0.0
HS35MOD	NA	NA	0	2.50000000E-1	-4.00000009E-9
HS76	NA	NA	0	-4.68181818	0.0
KSIP	NA	NA	0	5.75797941E-1	0.0
QPCBLEND	5.66E-16	8.94E-15	0	-7.84254307E-3	-2.74145844E-7
QPCBOEI1	2.05E-6	9.58E-6	0	1.15039140E+7	0.0
QPCBOEI2	3.42E-6	1.37E-5	0	8.17196224E+6	-1.22369628E-9
QPCSTAIR	4.34E-7	6.01E-6	0	6.20438745E+6	-4.83528799E-9
S268	NA	NA	0	-5.47370291E-8	-1.09550926
MOSARQP2	NA	NA	—	OOME[g]	—

[a]Mean of the absolute values of the components of ECE (Equality Constraint Error)
[b]Maximum of the absolute values of the components of ECE
[c]Total number of violated inequality constraints
[d]Minimum objective function value as computed by QuadProgJ
[e]Relative difference [f*-fBPMPD]/|fBPMPD| between the QuadProgJ and BPMPD solution values for the minimized objective function. A negative value indicates QuadProgJ improves on BPMPD.
[f]NA indicates "Not Applicable," meaning there are no constraints of the indicated type.
[g]Out-of-Memory Error indicated by a run-time Java Exception: java.lang.OutOfMemoryError

function value fBPMPD obtained by BPMPD, with no indication that the QuadProgJ solution x^* violates any equality or inequality constraints.[20]

Even in cases in which QuadProgJ improves on the BPMPD solution, however, the relative difference between the two solutions tends to be extremely small, generally on the order of 10^{-7}. The only exceptions are the two cases HS268 and S268 where QuadProgJ appears to improve significantly on the BPMPD solver. HS268 and S268 are relatively simple SCQP minimization problems subject only to inequality constraints, none of which turns out to be binding at the optimal solution. Why the interior-point BPMPD solver appears to degrade in accuracy on such problems is unclear.

All in all, QuadProgJ either matches or improves on the BPMPD solutions for all of the small and medium-sized SCQP test cases reported in Table 4, i.e. for all of the test cases

[20]Maros and Meszaros (1997) do not provide constraint checks for the BPMPD solutions reported in their repository.

for which TN (the total number of constraints plus decision variables) is less than 1500. Since the BPMPD solver has been in use since 1998, and is considered to have a proven high quality for solving QP problems, this finding suggests that QuadProgJ is at least as accurate a solver as BPMPD for SCQP problems of this size.

As noted previously, however, QuadProgJ is not designed for large-scale problems. The test results presented in Table 4 show that an out-of-memory error was triggered when an attempt was made to use QuadProgJ to solve test case MOSARQP2 with size TN = 1500. Whether this finding reflects an intrinsic limitation of QuadProgJ or is simply a desktop limitation that could be ameliorated by installing additional memory or by using a different hardware platform is an issue requiring further study.

8 DC OPF Test Case Results

8.1 Overview

In this section, QuadProgJ is used to solve illustrative three-node and five-node DC OPF test cases taken from power systems texts and ISO-NE/PJM training manuals.

Each of these DC OPF test cases is solved by invoking QuadProgJ through the outer Java shell DCOPFJ. Specifically, given SI input data and base apparent power and base voltage values as detailed in Section 6, DCOPFJ invokes QuadProgJ to solve for optimal real power injections, real power branch flows, voltage angles, LMPs, total variable costs, and various other output values. In particular, DCOPFJ automates the conversion of SI data to pu form for internal calculations and forms all needed matrix/vector representations.

These illustrative DC OPF test cases raise intriguing economic issues concerning the ISO operation of wholesale power markets in the presence of constraints on branch flows and production levels. The information content of LMPs in relation to these constraints is of particular interest. For the study at hand, however, these test cases are simply used to illustrate concretely the capability of QuadProgJ to generate detailed DC OPF solution values. The systematic study and interpretation of DC OPF solutions generated via QuadProgJ in the context of carefully constructed experimental designs is left for future studies.

The section concludes with a separate reporting of sensitivity results for the soft penalty weight $\pi > 0$ for both the three-node and five-node DC OPF test cases. These results demonstrate that the DC OPF solution values depend on the value of π in the expected way. The magnitude of the summed voltage angle differences is inversely related to the magnitude of π. However, for sufficiently small π the sensitivity of the DC OPF solution values to further decreases in π becomes negligible. Moreover, no numerical instability or convergence problems were detected at any of these tested π values.

8.2 Three-Node Test Results

Table 5 provides SI input as well as base apparent power and base voltage levels S_o and V_o for a day-ahead wholesale power market operating over a three-node transmission grid as depicted in Figure 1. The daily (24 hour) load distribution for the day-ahead market is

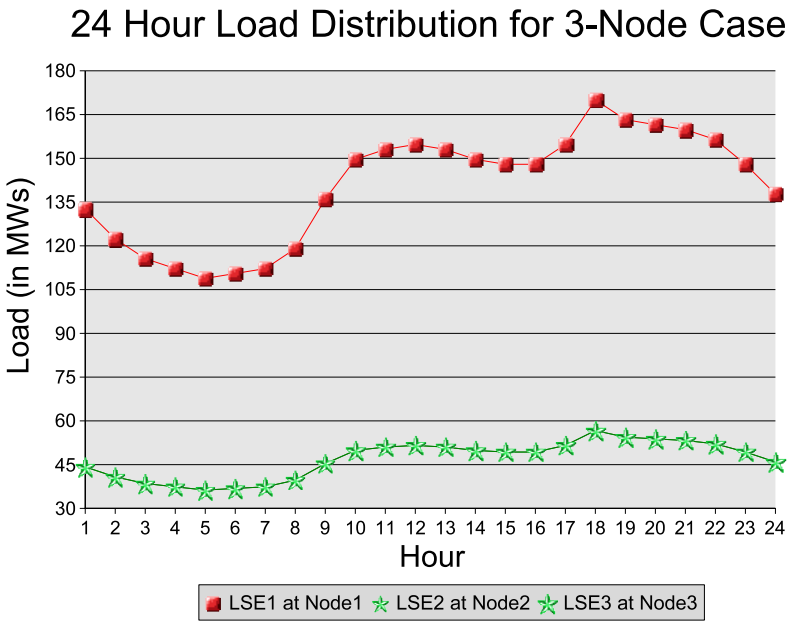

Figure 3: 24 Hour Load Distribution for a 3-Node Case

depicted in Figure 3. Note that LSE 2 and LSE 3 have identical load profiles. In addition, Generator 1 has the least expensive cost (as measured by the cost attributes a and b), and Generator 2's cost is between the cost of Generator 1 and Generator 3. This input data is adopted from Tables 8.2-8.4 (p. 297) in Shahidehpour et al. (2002).[21]

Tables 6-7 present DC OPF solution results in SI units for this day-ahead market for 24 successive hours. Specifically, Table 6 reports solution values for the real power injection p^*_{Gi} for each Generator i, the optimal voltage angle δ^*_k for each non-reference node k, and the LMP (λ^*_{eqk}/S_o) for each node k. Table 7 reports solution values for the twelve inequality constraint multipliers, the first six corresponding to thermal limits on branch flows and the final six corresponding to lower and upper bounds on production levels. Also reported in this table are the solution values for real power branch flows.

As seen in Table 7, the branch flow multipliers are all zero. This means there are no binding branch flow constraints, hence no branch congestion that would force higher-cost Generators to be dispatched prior to lower-cost Generators. Consequently, one would expect to see Generator 1 used to meet load demand as much as possible. Generator 2 should only produce more than its minimum production level when the load demand is so high that it exceeds the maximum production level of Generator 1, and Generator 3 should only produce

[21] Unfortunately, Shahidehpour et al. (2002) do not provide corresponding DC OPF solution values that could be used to compare against QuadProgJ solution values. Their focus is on the derivation of unit commitment schedules subject to additional security constraints that help to ensure reliability in the event of line outages.

more than its minimum production level when load demand is so high that it exceeds the maximum production level of Generator 2.

The solution results reported in Table 6 are consistent with these theoretical predictions. Examining the output columns for p^*_{G1}, p^*_{G2}, and p^*_{G3}, one sees the following pattern. For the low-demand off-peak hours (i.e. hours 02-08), Generator 1 is supplying as much of the load as possible; Generator 2 and Generator 3 are producing at their minimum production levels (10 MWs and 5 MWs, respectively). In contrast, for the high-demand peak hours (i.e. hours 01 and 09-24), Generator 1 is producing at its maximum production level (200 MWs) and Generator 2's production exceeds its minimum production level (10Mws). This clearly shows that dispatch priority is being based on cost attributes.

The column "minTVC" in Table 6 reports minimized total variable cost for each hour summed across all Generators. For the three-node example at hand, which has three Generators,

$$\text{minTVC} \;=\; \sum_{i=1}^{3} [a_i \cdot p^*_{Gi} + b_i \cdot p^{*2}_{Gi}] \tag{98}$$

As expected, minTVC changes hour by hour to reflect changes in the corresponding load; compare the daily load profile depicted in Figure 3.

Another important consistency check follows from the observation, made above, that all of the branch flow multipliers in Table 7 are zero, indicating the absence of any branch congestion. The absence of branch congestion implies that the LMPs should be the same across all nodes for each hour. This is verified by output columns LMP_1, LMP_2, and LMP_3 in Table 6.

Finally, Table 7 reports six multiplier values corresponding to six real power production constraints, two (lower and upper) for each of the three Generators. These multiplier values are entirely consistent with the results in Table 6. For example, the multiplier value associated with the minimum (lower) production level for Generator 3 is strictly positive for each hour, which is consistent with the result in Table 6 that Generator 3 is scheduled to produce at its minimum production level (5 MWs) for each hour.

8.3 Five-Node Test Results

Table 8 presents SI input data for a day-ahead wholesale power market operating over a five-node transmission grid as depicted in Figure 2.[22] The daily (24 hour) load distribution in SI units for the day-ahead market is depicted in Figure 4. Tables 9-13 report the optimal solution values in SI units for real power production levels, voltage angles, LMP values, minimum total variable cost, inequality constraint multipliers, and branch flows for 24 successive hours in the day-ahead market.

In contrast to the three-node case, this five-node case exhibits branch congestion. Specifically, branch congestion occurs between node 1 and node 2 (and only these nodes) in each

[22]The transmission grid, reactances, and locations of Generators and LSEs for this 5-node example are adopted from an example developed by John Lally (2002) for the ISO-NE that is now included in training manuals prepared by the ISO-NE (2007) and PJM (2007). The general shape of the LSE load profiles is adopted from a 3-node example presented in Shahidehpour et al. (2002, pp. 296-297).

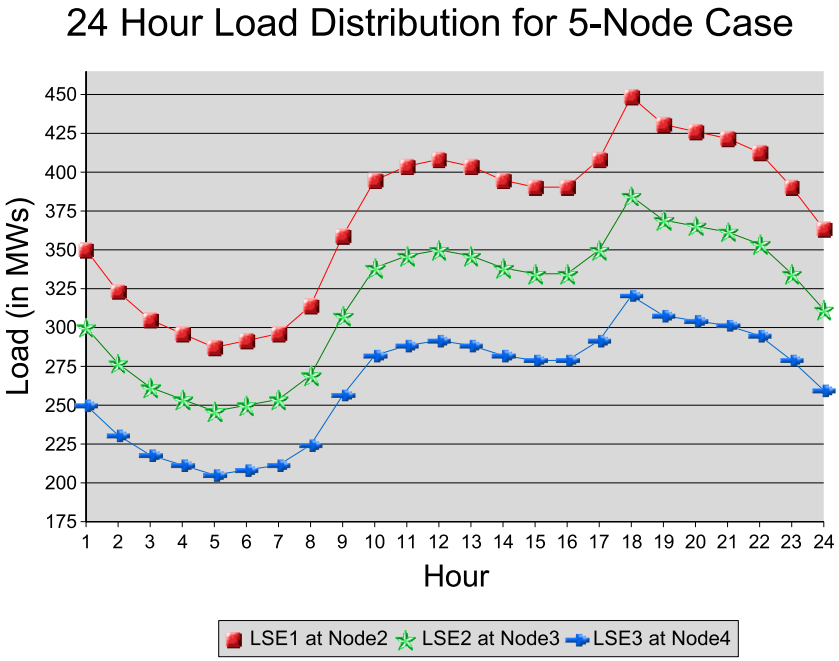

Figure 4: 24 Hour Load Distribution for a 5-Node Case

of the 24 hours. This can be verified directly by column P_{12} in Table 13, which shows that the real power flow P_{12} on branch $km = 12$ is at its upper thermal limit (250 MWs) for each hour. It can also be verified indirectly by column "12" in Table 11, which shows that the thermal inequality constraint multiplier for branch $km = 12$ is positively valued for each hour, indicating a binding constraint. The direct consequence of this branch congestion is the occurrence of widespread LMP separation, i.e. the LMP values differ across all nodes for each hour. This can be verified by examining output columns LMP_1-LMP_5 in Table 10.

Examining this LMP data more closely, it is seen that LMP_2 and LMP_3 (the LMPs for nodes 2 and 3) exhibit a sharp change in hour 18, increasing between hour 17 and hour 18 by about 100% and then dropping back to "normal" levels in hour 19 and beyond. Interesting, this type of sudden spiking in LMP values is also observed empirically in MISO's Dynamic LMP Contour Map[23] for real-time market prices, which is updated every five minutes.

This rather dramatic LMP peaking in hour 18 can be traced to several factors. First, as seen in Figure 4, the load profile for each LSE peaks at hour 18. Second, when solving the DC OPF problem to meet the high load in hour 18, the ISO has to take into consideration the maximum production limit for Generator 3 as well as the thermal inequality constraint between node 1 and node 2. Both of these constraints turn out to be binding. Specifically, as seen in Table 9, Generator 3 is dispatched in hour 18 at its maximum production limit (520 MWs); and, as seen in Table 13, the real power flow in branch $km = 12$ is at its upper

[23]http://www.midwestmarket.org/page/LMP%20Contour%20Map%20&%20Data

limit (250 MWs) for all 24 hours. Given the configuration of the transmission grid, to meet the hour 18 peak load the ISO is forced to back down (relative to hour 17) the less expensive production of Generators 1 and 2 and to use instead the more expensive production of the "peaker" Generator 4.

After the peak hour 18, the load returns to lower levels. The ISO is then able to dispatch Generator 1 and Generator 2 at their more "normal" levels, with Generator 1 at its upper production limit, and to avoid dispatching any production from generation 4; note from Table 8 that the minimum production level of Generator 4 is 0. Furthermore, the LMPs drop back to their more normal levels after hour 18.

8.4 Π Sensitivity Test Results

Sensitivity tests were conducted to check the extent to which the solution values reported in Sections 8.2 and 8.3 for the three-node and five-node DC OPF test cases depend on the specific choice of the soft penalty weight π.

For the three-node case, a separate solution set was generated for each of the following five π values: 100, 10, 1, 0.1 and 0.01. These five solution sets are reported in Tables 14-18. These solution results show that decreasing the value of π over the tested range from 100 to 0.01 had little impact on the resulting solution values. The only perceptible changes at the reported precision level (four decimal places) were in the LMP values in their second and higher decimal places. Moreover, the LMP values stabilized through two decimal places (i.e. to values rounded off to pennies) once π decreased to the level 1.0.

Tables 19 and 20 report the sum of squared voltage angle differences for the three-node and five-node DC OPF test cases as the soft penalty weight π is decreased in value from 100 to 0.01. As can be seen, the maximum absolute differences (MaxAD) between these sums are extremely small: namely, about 10^{-15} in magnitude for the three-node case and about 10^{-7} in magnitude for the five-node case. In the three-node case, any change in these sums in response to the changes in the value of π are below visibility in the reported data. In the five-node case, however, the sums are seen to increase slightly as the value of π decreases, which is the expected result of decreasing the penalty attached to the sum.

Also as expected, the sum of squared voltage angle differences increases with an increase in nodes from three to five for each tested value of π. This suggests that a researcher might need to tailor the value of π to the problem at hand in order to achieve a desired degree of smallness for voltage angle differences. In addition, in some situations it might be desirable to introduce individual weights on the voltage angle differences instead of using a common weight π, e.g. in order to represent transmission grid losses. This could easily be accomplished by a simple respecification of the weight matrix $\mathbf{W}$ in (43).

9 Concluding Remarks

Restructured electricity markets are extraordinarily complex. For example, restructured wholesale power markets in the U.S. typically involve spot and forward energy markets operated by ISO/RTOs over AC transmission grids subject to congestion effects. As reported

by Joskow (2006, Table 1), over 50% of the generation capacity in the U.S. is now operating under this market design, and other regions of the U.S. are moving towards this form of organization.

The complexity of restructured electricity markets essentially forces electricity researchers to resort to computational methods of analysis. Unfortunately, much of the software currently available for computational electricity modeling is commercial and hence proprietary. This restricts the ability of electricity researchers to publish self-sufficient studies permitting full access to implementation.

A key stumbling block to developing open-source software for general academic research into restructured electricity markets is the need to model the AC/DC optimal power flow (OPF) problems that must repeatedly be solved by ISO/RTO operators in order to generate daily unit commitment and dispatch schedules, as well as locational marginal prices (LMPs), for both spot and forward energy markets. Developing algorithms for the successful solution of optimization problems involving mixed collections of equality and inequality constraints, even when specialized to quadratic objective functions (as in DC OPF approximations to AC OPF problems), is a daunting task full of pitfalls for the unwary.

This study reports the development of QuadProgJ, an open-source plug-and-play Java solver for strictly convex quadratic programming (SCQP) problems that can be applied to standard DC OPF problems for research and training purposes. QuadProgJ implements the well-known dual active-set SCQP algorithm developed by Goldfarb and Idnani (1983). The accuracy of QuadProgJ is demonstrated by means of comparative results for a well-known suite of QP test problems with up to 1500 decision variables plus constraints.

In addition, this study proposes a physically meaningful augmentation of the standard DC OPF problem that permits the direct generation of solution values for LMPs, voltage angles, and voltage angle differences together with real power injections and branch flows. Three-node and five-node test cases are used to demonstrate how QuadProgJ, coupled with a Java outer shell DCOPFJ, can be used to directly generate complete solution values for this augmented DC OPF problem. In particular, DCOPFJ automates the SI/pu conversion and matrix/vector representation of all needed input data for this augmented DC OPF problem.

Appendix A: Derivation of Power Flow Branch Equations

Recall from Section 3.1 that equations for the flow of real and reactive power in any transmission grid branch km ($k \neq m$) are depicted as follows:

$$P_{km} = V_k^2 g_{km} - V_k V_m [g_{km} \cos(\delta_k - \delta_m) + b_{km} \sin(\delta_k - \delta_m)] \tag{99}$$

$$Q_{km} = -V_k^2 b_{km} - V_k V_m [g_{km} \sin(\delta_k - \delta_m) - b_{km} \cos(\delta_k - \delta_m)] \tag{100}$$

This appendix provides a rigorous derivation of these equations from Ohm's Law.

A.1 Preliminary: The Relationship Between Impedance and Admittance

Using standard notational conventions, the impedance z on a transmission grid branch is expressed as

$$z = r + jx \qquad \text{(impedance = resistance + } \sqrt{-1} \text{ reactance)} \tag{101}$$

and the admittance y on a transmission grid branch is expressed as

$$y = g + jb \qquad \text{(admittance = conductance + } \sqrt{-1} \text{ susceptance)} \tag{102}$$

Since $y = 1/z$, it follows that

$$y \;=\; \frac{1}{z} \;=\; \frac{1}{r + jx} \;=\; \frac{r}{r^2 + x^2} \;+\; j\,\frac{-x}{r^2 + x^2} \tag{103}$$

Thus,

$$g = \frac{r}{r^2 + x^2}$$

$$b = \frac{-x}{r^2 + x^2}$$

A.2 Derivation of Equations (99) and (100)

The following derivation[24] is based on Gönen (1988, (2.4)). Boldface letters denote complex variables while letters in normal font denote real variables. Also, the following trigonometric identities will be used in this derivation:

$$\cos(\alpha - \beta) = \cos\alpha\cos\beta + \sin\alpha\sin\beta$$

$$\sin(\alpha - \beta) = \sin\alpha\cos\beta - \cos\alpha\sin\beta$$

Let km denote any transmission grid branch, and let $\mathbf{S}_{km}$ (in MVA) denote the complex power flowing in this branch. This complex power can be represented as

$$\mathbf{S_{km}} = P_{km} + jQ_{km} = \mathbf{V_k I^*_{km}} \tag{104}$$

where

$$j = \sqrt{-1}$$

$$\mathbf{V_k} = V_k\cos\delta_k + jV_k\sin\delta_k$$

$$\mathbf{I_{km}} \;=\; \text{Current (in Amperes) on branch } km$$

$$\mathbf{I^*_{km}} = \text{Complex conjugate of } \mathbf{I_{km}}$$

By Ohm's Law in AC settings,

[24] Recall from Section 2.2 that all transformer tap ratios are assumed to be 1, and all transformer phase angle shifts and line-charging capacitances are assumed to be 0. For an alternative derivation of the power flow equations that permits general settings for these variables, see Hogan (2002, Appendix).

$$\mathbf{I_{km}} = \frac{\mathbf{V_k} - \mathbf{V_m}}{\mathbf{z_{km}}} \tag{105}$$

where the impedance $\mathbf{z_{km}}$ on branch km can be expressed as

$$\mathbf{z_{km}} = r_{km} + jx_{km}$$

The complex conjugate of the impedance $\mathbf{z_{km}}^*$ is then written as

$$\mathbf{z^*_{km}} = r_{km} - jx_{km}$$

Consequently, $\mathbf{S_{km}}$ can be written as:

$$\begin{aligned}
\mathbf{S_{km}} &= \mathbf{V_k}\frac{\mathbf{V_k^*} - \mathbf{V_m^*}}{\mathbf{z_{km}^*}} \\
&= [V_k\cos\delta_k + jV_k\sin\delta_k]\frac{[V_k\cos\delta_k - jV_k\sin\delta_k] - [V_m\cos\delta_m - jV_m\sin\delta_m]}{r_{km} - jx_{km}} \\
&= \frac{[V_k^2\cos^2\delta_k + V_k^2\sin^2\delta_k] - V_k[\cos\delta_k + j\sin\delta_k]V_m[\cos\delta_m - j\sin\delta_m]}{r_{km} - jx_{km}} \\
&= \frac{V_k^2 - V_kV_m\left[(\cos\delta_k\cos\delta_m + \sin\delta_k\sin\delta_m) + j(\sin\delta_k\cos\delta_m - \cos\delta_k\sin\delta_m)\right]}{r_{km} - jx_{km}} \\
&= \frac{V_k^2 - V_kV_m[\cos(\delta_k - \delta_m) + j\sin(\delta_k - \delta_m)]}{r_{km} - jx_{km}} \qquad (\text{Let } \theta = \delta_k - \delta_m) \\
&= \frac{[r_{km} + jx_{km}]V_k^2 - [r_{km} + jx_{km}]V_kV_m[\cos\theta + j\sin\theta]}{[r_{km} + jx_{km}][r_{km} - jx_{km}]} \\
&= \frac{r_{km}V_k^2 - V_kV_m[r_{km}\cos\theta - x_{km}\sin\theta]}{r_{km}^2 + x_{km}^2} + j\frac{x_{km}V_k^2 - V_kV_m[r_{km}\sin\theta + x_{km}\cos\theta]}{r_{km}^2 + x_{km}^2} \\
&= \left(V_k^2g_{km} - V_kV_m[g_{km}\cos\theta + b_{km}\sin\theta]\right) + j\left(-V_k^2b_{km} - V_kV_m[g_{km}\sin\theta - b_{km}\cos\theta]\right) \\
&= P_{km} + jQ_{km}
\end{aligned}$$

Hence, we can infer that (99) and (100) hold.

Appendix B: Expressing DC OPF Voltage Angles as a Linear Affine Function of Real Power Injections

This section establishes that the vector δ of non-reference voltage angles $(\delta_2, \ldots, \delta_K)^T$ in the standard DC OPF problem in pu form presented in Section 3.2 can be expressed as a linear affine function of the vector of real power injections.

The basic equations to consider are the real power nodal balance constraints (26) for $k = 2, \ldots, K$ together with the normalization $\delta_1 = 0$ imposed on the reference node voltage angle δ_1 by constraint (33). When the nodal balance constraint for any node $k \geq 2$ is expressed solely in terms of voltage angles, real power injections, and real power loads, it takes the following form:

$$\sum_{i \in I_k} P_{Gi} - \sum_{km \text{ or } mk \in BR} B_{km}[\delta_k - \delta_m] \;=\; \sum_{j \in J_k} P_{Lj} \tag{106}$$

This collection of nodal balance constraints for $k = 2, \ldots, K$ can equivalently be expressed in matrix form as follows:

$$\mathbf{PNetInject} = \mathbf{B'_{rr}}\delta \tag{107}$$

where **PNetInject** denotes the $(K-1) \times 1$ vector of net nodal real power injections PNetInject_k for nodes $k = 2, \ldots, K$, and $\mathbf{B'_{rr}}$ denotes the bus admittance matrix $\mathbf{B'}$ in (51) with its first row and first column eliminated (corresponding to the reference node 1). For concrete illustration, equation (107) for the 5-node test case presented in Section 5.2 takes the following specific form:

$$\begin{bmatrix} 0 - P_{L1} \\ P_{G3} - P_{L2} \\ P_{G4} - P_{L3} \\ P_{G5} - 0 \end{bmatrix} = \begin{bmatrix} B_{21} + B_{23} & -B_{23} & 0 & 0 \\ -B_{32} & B_{32} + B_{34} & -B_{34} & 0 \\ 0 & -B_{43} & B_{41} + B_{43} + B_{45} & -B_{45} \\ 0 & 0 & -B_{54} & B_{51} + B_{54} \end{bmatrix}_{4\times 4} \begin{bmatrix} \delta_2 \\ \delta_3 \\ \delta_4 \\ \delta_5 \end{bmatrix} \tag{108}$$

Since the matrix $\mathbf{B'_{rr}}$ is invertible by construction, we have the following relationship between the voltage angles and the net nodal power injections:

$$\delta = [\mathbf{B'_{rr}}]^{-1}\mathbf{PNetInject} \tag{109}$$

In terms of the 5-node test case, equation (109) takes the following form:

$$\begin{bmatrix} \delta_2 \\ \delta_3 \\ \delta_4 \\ \delta_5 \end{bmatrix} = \begin{bmatrix} B_{21} + B_{23} & -B_{23} & 0 & 0 \\ -B_{32} & B_{32} + B_{34} & -B_{34} & 0 \\ 0 & -B_{43} & B_{41} + B_{43} + B_{45} & -B_{45} \\ 0 & 0 & -B_{54} & B_{51} + B_{54} \end{bmatrix}^{-1}_{4\times 4} \begin{bmatrix} 0 - P_{L1} \\ P_{G3} - P_{L2} \\ P_{G4} - P_{L3} \\ P_{G5} - 0 \end{bmatrix} \tag{110}$$

The net nodal power injection vector **PNetInject** can be further decomposed into a linear affine function of the real power injection vector $\mathbf{P_G} = (P_{G1}, \ldots, P_{GI})^T$ as follows:

$$\mathbf{PNetInject} = \mathbf{R}\mathbf{P_G} + \beta \tag{111}$$

where $\mathbf{R}$ is a $(K-1) \times I$ matrix and β is a $(K-1) \times 1$ vector defined as follows

$$\mathbf{R} = \begin{bmatrix} \mathbb{I}(1 \in I_2) & \mathbb{I}(2 \in I_2) & \cdots & \mathbb{I}(I \in I_2) \\ \mathbb{I}(1 \in I_3) & \mathbb{I}(2 \in I_3) & \cdots & \mathbb{I}(I \in I_3) \\ \vdots & \vdots & \ddots & \vdots \\ \mathbb{I}(1 \in I_K) & \mathbb{I}(2 \in I_K) & \cdots & \mathbb{I}(I \in I_K) \end{bmatrix}_{(K-1)\times I} \tag{112}$$

where

$$\mathbb{I}(i \in I_k) = \begin{cases} 1 & \text{if } i \in I_k \\ 0 & \text{if } i \notin I_k \end{cases}$$

$$\beta = \begin{bmatrix} -\sum_{j\in J_2} P_{Lj} & -\sum_{j\in J_3} P_{Lj} & \cdots & -\sum_{j\in J_K} P_{Lj} \end{bmatrix}^T_{(K-1)\times 1} \tag{113}$$

Again using the 5-node test case for concrete illustration, we can write out equation (111) as

$$\begin{bmatrix} 0 - P_{L1} \\ P_{G3} - P_{L2} \\ P_{G4} - P_{L3} \\ P_{G5} - 0 \end{bmatrix} = \begin{bmatrix} 0 & 0 & 0 & 0 & 0 \\ 0 & 0 & 1 & 0 & 0 \\ 0 & 0 & 0 & 1 & 0 \\ 0 & 0 & 0 & 0 & 1 \end{bmatrix} \begin{bmatrix} P_{G1} \\ P_{G2} \\ P_{G3} \\ P_{G4} \\ P_{G5} \end{bmatrix} + \begin{bmatrix} -P_{L1} \\ -P_{L2} \\ -P_{L3} \\ 0 \end{bmatrix} \tag{114}$$

Finally, combining (109) and (111), we see that it is possible to solve explicitly for the voltage angle vector δ as a linear affine function of the real power injection vector $\mathbf{P_G}$: namely,

$$\delta = \mathbf{R}^* \mathbf{P_G} + \nu \tag{115}$$

where $\mathbf{R}^* = [\mathbf{B}'_{\mathbf{rr}}]^{-1}\mathbf{R}$ and $\nu = [\mathbf{B}'_{\mathbf{rr}}]^{-1}\beta$.

References

Anderson, Paul. M. (1995), *Analysis of Faulted Power Systems*, Wiley-IEEE Press, New York.

Boland, Natashia L. (1997), "A Dual-Active-Set Algorithm for Positive Semi-Definite Quadratic Programming," *Mathematical Programming* 78, 1-27.

CAISO (2003), "Locational Marginal Pricing (LMP) Study: Analysis of Cost-Based Differentials," *Market Design 2002*, CAISO Market Operations, California ISO, February 4 release.

FERC (2003), *Notice of White Paper*, U.S. Federal Energy Regulatory Commission, Issued April 28.

Fletcher, Roger (1987), *Practical Methods of Optimization*, Second Edition, John Wiley & Sons, New York.

Goldfarb, Donald, and Ashok Udhawdas Idnani (1983), "A Numerically Stable Dual Method for Solving Strictly Convex Quadratic Programs," *Mathematical Programming* 27, 1-33.

Gönen, Turan (1988), *Modern Power System Analysis*, Wiley-Interscience, John Wiley & Sons, Inc., New York.

Hogan, William W. (2002), "Financial Transmission Rights Formulations," Report, Center for Business and Government, John F. Kennedy School of Government, Harvard University, Cambridge, MA.

ISO-NE (2007), Home Page, ISO New England, Inc., accessible at http://www.iso-ne.com/

ISO-NE (2003), Standard Market Design Reference Guide, ISO New England, Inc., 45pp. Available at http://www.iso-ne.com/smd/

Joskow, Paul (2006), "Markets for Power in the United States: An Interim Assessment," *The Energy Journal*, Vol. 27(1), 1-36.

Kirschen, Daniel S., and Goran Strbac (2004), *Fundamentals of Power System Economics*, John Wiley & Sons, Ltd.

Koesrindartoto, Deddy, and Leigh Tesfatsion (2004), "Testing the Economic Reliability of FERC's Wholesale Power Market Platform: An Agent-Based Computational Approach," *Energy, Environment, and Economics in a New Era*, Proceedings of the 24th USAEE/IAEE North American Conference, Washington, D.C., July 8-10.

Koesrindartoto, Deddy, Junjie Sun, and Leigh Tesfatsion (2005), "An Agent-Based Computational Laboratory for Testing the Economic Reliability of Wholesale Power Market Designs," *Proceedings*, Vol. 1, IEEE Power Engineering Society General Meeting, San Francisco, CA, June 2005, pp. 931-936.

Lally, John (2002), "Financial Transmission Rights: Auction Example," Section 6, M-06 Financial Transmission Rights Draft 01-10-02, ISO New England, Inc., January.

Maros, Istvan, and Csaba Meszaros (1997), "A Repository of Convex Quadratic Programming Problems," Department Technical Report DOC 97/6, Department of Computing, Imperial College, London, U.K.

McCalley, James D. (2006), "The Power Flow Equations," Lecture Notes, Department of Electrical Engineering, Iowa State University.

MISO (2007), Home Page, Midwest ISO, Inc., accessible at http://www.midwestiso.org/

Overbye, Thomas J., Xu Cheng, and Yan Sun (2004), "A Comparison of the AC and DC Power Flow Models for LMP Calculations," *Proceedings*, 37th Hawaii International Conference on System Sciences. http://csdl.computer.org/comp/proceedings/hicss/

PJM (2007), PJM Home Page, accessible at www.pjm.com .

Powell, Michael J. D. (1983), "ZQPCVX: A Fortran Subroutine for Convex Quadratic Programming," Techical Report DAMTP/1983/NA17, Department of Applied Mathematics and Theoretical Physics, University of Cambridge, England.

Shahidehpour, Mohammad, Hatim Yamin, and Zuyi Li (2002), *Market Operations in Electric Power Systems*, IEEE/Wiley-Interscience, John Wiley & Sons, Inc., New York.

Stoer, Josef (1992), "A Dual Algorithm for Solving Degenerate Linearly Constrained Linear Least Squares Problems," *Journal of Numerical Linear Algebra with Applications* 1, 103-131.

Sun, Junjie and Leigh Tesfatsion (2007), "Dynamic Testing of Wholesale Power Market Designs: An Agent-Based Computational Approach", Economics Working Paper No. 06025, Iowa State University, revised June.
Available at: http://www.econ.iastate.edu/tesfatsi/DynTestAMES.JSLT.pdf

Wood, Allen J., and Bruce F. Wollenberg (1996), *Power Generation, Operation, and Control*, Second Edition, John Wiley & Sons, Inc., New York.

Table 5: DC OPF Input Data in SI Units for Three-Node Case

Base Values[a]

S_o	V_o
100	10

K[b]	π[c]
3	0.05

Branch

From	To	lineCap[d]	x[e]
1	2	55	0.20
1	3	55	0.40
2	3	55	0.25

Gen

ID	atNode	FCost	a	b	pMin[f]	pMax[g]
1	1	14	10.6940	0.00463	20	200
2	2	21	18.1000	0.00612	10	150
3	3	11	37.8896	0.01433	5	20

LSE

ID	atNode	L-00[h]	L-01	L-02	L-03	L-04	L-05	L-06	L-07
1	1	132.66	122.4	115.62	112.2	108.84	110.52	112.2	119.04
2	2	44.22	40.8	38.54	37.4	36.28	36.84	37.4	39.68
3	3	44.22	40.8	38.54	37.4	36.28	36.84	37.4	39.68
ID	atNode	L-09	L-10	L-11	L-12	L-13	L-14	L-15	L-16
1	1	136.02	149.64	153.06	154.74	153.06	149.64	147.96	147.96
2	2	45.34	49.88	51.02	51.58	51.02	49.88	49.32	49.32
3	3	45.34	49.88	51.02	51.58	51.02	49.88	49.32	49.32
ID	atNode	L-17	L-18	L-19	L-20	L-21	L-22	L-23	L-24
1	1	154.74	170.04	163.26	161.52	159.84	156.42	147.96	137.76
2	2	51.58	56.68	54.42	53.84	53.28	52.14	49.32	45.92
3	3	51.58	56.68	54.42	53.84	53.28	52.14	49.32	45.92

[a]The base voltage V_o is measured in kVs and the base apparent power S_o is measured in MVAs. For illustrative purposes, S_o and V_o are chosen such that the base impedance Z_o satisfies $Z_o = V_o^2/S_o = 1$

[b]Total number K of nodes

[c]Soft penalty weight π for voltage angle differences

[d]Upper limit P_{km}^U (in MWs) on magnitude of real power flow in branch km

[e]Reactance x_{km} (in ohms) for branch km

[f]Lower limit p_{Gi}^L (in MWs) on real power production for Generator i

[g]Upper limit p_{Gi}^U (in MWs) on real power production for Generator i

[h]L-H: Load (in MWs) for hour H, where H=00,02,...,23

Table 6: DC OPF Solution Results in SI Units for Three-Node Case

Hour	p^*_{G1}	p^*_{G2}	p^*_{G3}	$\delta^{*\,a}_2$	δ^*_3	$\text{LMP}_1{}^b$	LMP_2	LMP_3	minTVC^c
01	200.0	16.1	5.0	-0.0799	-0.1095	18.30	18.30	18.30	2993.95
02	189.0	10.0	5.0	-0.0808	-0.1048	12.44	12.44	12.44	2724.33
03	177.7	10.0	5.0	-0.0752	-0.0979	12.34	12.34	12.34	2565.12
04	172.0	10.0	5.0	-0.0724	-0.0944	12.29	12.29	12.29	2485.70
05	166.4	10.0	5.0	-0.0696	-0.0910	12.23	12.23	12.23	2408.27
06	169.2	10.0	5.0	-0.0710	-0.0927	12.26	12.26	12.26	2446.91
07	172.0	10.0	5.0	-0.0724	-0.0944	12.29	12.29	12.29	2485.70
08	183.4	10.0	5.0	-0.0780	-0.1014	12.39	12.39	12.39	2645.13
09	200.0	21.7	5.0	-0.0741	-0.1077	18.37	18.37	18.37	3097.90
10	200.0	44.4	5.0	-0.0506	-0.1002	18.64	18.64	18.64	3527.13
11	200.0	50.1	5.0	-0.0447	-0.0983	18.71	18.71	18.71	3636.90
12	200.0	52.9	5.0	-0.0418	-0.0974	18.75	18.75	18.75	3691.11
13	200.0	50.1	5.0	-0.0447	-0.0983	18.71	18.71	18.71	3636.90
14	200.0	44.4	5.0	-0.0506	-0.1002	18.64	18.64	18.64	3527.13
15	200.0	41.6	5.0	-0.0535	-0.1011	18.61	18.61	18.61	3473.51
16	200.0	41.6	5.0	-0.0535	-0.1011	18.61	18.61	18.61	3473.51
17	200.0	52.9	5.0	-0.0418	-0.0974	18.75	18.75	18.75	3691.11
18	200.0	78.4	5.0	-0.0154	-0.0890	19.06	19.06	19.06	4193.64
19	200.0	67.1	5.0	-0.0271	-0.0927	18.92	18.92	18.92	3968.98
20	200.0	64.2	5.0	-0.0301	-0.0937	18.89	18.89	18.89	3911.83
21	200.0	61.4	5.0	-0.0330	-0.0946	18.85	18.85	18.85	3856.85
22	200.0	55.7	5.0	-0.0389	-0.0965	18.78	18.78	18.78	3745.51
23	200.0	41.6	5.0	-0.0535	-0.1011	18.61	18.61	18.61	3473.51
24	200.0	24.6	5.0	-0.0711	-0.1067	18.40	18.40	18.40	3152.03

[a]Voltage angle solutions δ^*_k are reported in radians

[b]Locational marginal price, $\text{LMP}_k = \lambda^*_{eqk}/S_o$ for each node k

[c]Minimized total variable cost

Table 7: DC OPF Solution Results in SI Units for Three-Node Case - Inequality Constraint Multipliers and Real Power Branch Flows

	Branch km multipliers						Production constraint multipliers						Branch Flow		
Hour	12	13	23	21	31	32	P^L_{G1}	P^L_{G2}	P^L_{G3}	P^U_{G1}	P^U_{G2}	P^U_{G3}	P_{12}	P_{13}	P_{23}
01	0	0	0	0	0	0	0	0	19.74	5.75	0	0	39.96	27.38	11.84
02	0	0	0	0	0	0	0	5.78	25.59	0	0	0	40.40	26.20	9.60
03	0	0	0	0	0	0	0	5.88	25.69	0	0	0	37.61	24.47	9.07
04	0	0	0	0	0	0	0	5.94	25.75	0	0	0	36.20	23.60	8.80
05	0	0	0	0	0	0	0	5.99	25.80	0	0	0	34.82	22.74	8.54
06	0	0	0	0	0	0	0	5.96	25.77	0	0	0	35.51	23.17	8.67
07	0	0	0	0	0	0	0	5.94	25.75	0	0	0	36.20	23.60	8.80
08	0	0	0	0	0	0	0	5.83	25.64	0	0	0	39.02	25.34	9.34
09	0	0	0	0	0	0	0	0	19.67	5.82	0	0	37.06	26.92	13.42
10	0	0	0	0	0	0	0	0	19.39	6.10	0	0	25.31	25.05	19.83
11	0	0	0	0	0	0	0	0	19.32	6.17	0	0	22.36	24.58	21.44
12	0	0	0	0	0	0	0	0	19.29	6.20	0	0	20.91	24.35	22.23
13	0	0	0	0	0	0	0	0	19.32	6.17	0	0	22.36	24.58	21.44
14	0	0	0	0	0	0	0	0	19.39	6.10	0	0	25.31	25.05	19.83
15	0	0	0	0	0	0	0	0	19.42	6.06	0	0	26.76	25.28	19.04
16	0	0	0	0	0	0	0	0	19.42	6.06	0	0	26.76	25.28	19.04
17	0	0	0	0	0	0	0	0	19.29	6.20	0	0	20.91	24.35	22.23
18	0	0	0	0	0	0	0	0	18.97	6.51	0	0	7.71	22.25	29.43
19	0	0	0	0	0	0	0	0	19.11	6.38	0	0	13.56	23.18	26.24
20	0	0	0	0	0	0	0	0	19.15	6.34	0	0	15.06	23.42	25.42
21	0	0	0	0	0	0	0	0	19.18	6.31	0	0	16.51	23.65	24.63
22	0	0	0	0	0	0	0	0	19.25	6.24	0	0	19.46	24.12	23.02
23	0	0	0	0	0	0	0	0	19.42	6.06	0	0	26.76	25.28	19.04
24	0	0	0	0	0	0	0	0	19.63	5.86	0	0	35.56	26.68	14.24
													P^U_{12}	P^U_{13}	P^U_{23}
													55	55	55

Table 8: DC OPF Input Data in SI Units for Five-Node Case

Base Values

S_o	V_o
100	10

K	π
5	0.05

Branch

From	To	lineCap	x
1	2	250	0.0281
1	4	150	0.0304
1	5	400	0.0064
2	3	350	0.0108
3	4	240	0.0297
4	5	240	0.0297

Gen

ID	atNode	FCost	a	b	pMin	pMax
1	1	16	14	0.005	0	110
2	1	19	15	0.006	0	100
3	3	28	25	0.010	0	520
4	4	10	30	0.012	0	200
5	5	24	10	0.007	0	600

LSE

ID	atNode	L-01	L-02	L-03	L-04	L-05	L-06	L-07	L-08
1	2	350.00	322.93	305.04	296.02	287.16	291.59	296.02	314.07
2	3	300.00	276.80	261.47	253.73	246.13	249.93	253.73	269.20
3	4	250.00	230.66	217.89	211.44	205.11	208.28	211.44	224.33
ID	atNode	L-09	L-10	L-11	L-12	L-13	L-14	L-15	L-16
1	2	358.86	394.80	403.82	408.25	403.82	394.80	390.37	390.37
2	3	307.60	338.40	346.13	349.93	346.13	338.40	334.60	334.60
3	4	256.33	282.00	288.44	291.61	288.44	282.00	278.83	278.83
ID	atNode	L-17	L-18	L-19	L-20	L-21	L-22	L-23	L-24
1	2	408.25	448.62	430.73	426.14	421.71	412.69	390.37	363.46
2	3	349.93	384.53	369.20	365.26	361.47	353.73	334.60	311.53
3	4	291.61	320.44	307.67	304.39	301.22	294.78	278.83	259.61

Table 9: DC OPF Solution Results in SI Units for Five-Node Case - Optimal Real Power Production Levels and Optimal Voltage Angles (in Radians)

Hour	p^*_{G1}	p^*_{G2}	p^*_{G3}	p^*_{G4}	p^*_{G5}	δ^*_2	δ^*_3	δ^*_4	δ^*_5
01	110.00	13.87	332.53	0.00	443.59	-0.0702	-0.0595	-0.0394	0.0164
02	110.00	13.44	269.41	0.00	437.54	-0.0702	-0.0624	-0.0385	0.0162
03	110.00	13.16	227.70	0.00	433.54	-0.0702	-0.0643	-0.0379	0.0161
04	110.00	13.01	206.66	0.00	431.52	-0.0703	-0.0653	-0.0376	0.0160
05	110.00	12.87	185.99	0.00	429.53	-0.0703	-0.0662	-0.0373	0.0160
06	110.00	12.95	196.33	0.00	430.53	-0.0702	-0.0658	-0.0375	0.0160
07	110.00	13.01	206.66	0.00	431.52	-0.0703	-0.0653	-0.0376	0.0160
08	110.00	13.30	248.75	0.00	435.55	-0.0703	-0.0633	-0.0382	0.0162
09	110.00	14.01	353.20	0.00	445.58	-0.0703	-0.0585	-0.0397	0.0164
10	110.00	14.58	437.00	0.00	453.61	-0.0702	-0.0546	-0.0409	0.0166
11	110.00	14.73	458.03	0.00	455.63	-0.0702	-0.0536	-0.0412	0.0167
12	110.00	14.80	468.37	0.00	456.62	-0.0702	-0.0532	-0.0413	0.0167
13	110.00	14.73	458.03	0.00	455.63	-0.0702	-0.0536	-0.0412	0.0167
14	110.00	14.58	437.00	0.00	453.61	-0.0702	-0.0546	-0.0409	0.0166
15	110.00	14.51	426.67	0.00	452.62	-0.0702	-0.0551	-0.0407	0.0166
16	110.00	14.51	426.67	0.00	452.62	-0.0702	-0.0551	-0.0407	0.0166
17	110.00	14.80	468.37	0.00	456.62	-0.0702	-0.0532	-0.0413	0.0167
18	2.07	0.00	520.00	108.88	522.63	-0.0702	-0.0488	-0.0300	0.0222
19	107.35	6.12	520.00	0.00	474.13	-0.0702	-0.0507	-0.0418	0.0175
20	110.00	15.08	510.08	0.00	460.63	-0.0702	-0.0512	-0.0419	0.0168
21	110.00	15.01	499.76	0.00	459.63	-0.0702	-0.0517	-0.0418	0.0168
22	110.00	14.87	478.71	0.00	457.62	-0.0702	-0.0527	-0.0415	0.0167
23	110.00	14.51	426.67	0.00	452.62	-0.0702	-0.0551	-0.0407	0.0166
24	110.00	14.09	363.91	0.00	446.60	-0.0702	-0.0580	-0.0399	0.0164

Table 10: DC OPF Solution Results in SI Units for Five-Node Case - LMP Values (Equality Constraint Multipliers) and Minimized Total Variable Cost

Hour	LMP_1	LMP_2	LMP_3	LMP_4	LMP_5	minTVC
01	15.17	35.50	31.65	21.05	16.21	19587.11
02	15.16	33.95	30.39	20.60	16.13	17107.25
03	15.16	32.92	29.55	20.30	16.07	15556.75
04	15.16	32.40	29.13	20.15	16.04	14800.93
05	15.15	31.89	28.72	20.00	16.01	14076.09
06	15.16	32.15	28.93	20.07	16.03	14436.48
07	15.16	32.40	29.13	20.15	16.04	14800.93
08	15.16	33.44	29.97	20.45	16.10	16330.20
09	15.17	36.01	32.06	21.20	16.24	20433.88
10	15.18	38.08	33.74	21.81	16.35	24043.63
11	15.18	38.60	34.16	21.96	16.38	24993.90
12	15.18	38.85	34.37	22.03	16.39	25467.47
13	15.18	38.60	34.16	21.96	16.38	24993.90
14	15.18	38.08	33.74	21.81	16.35	24043.63
15	15.17	37.82	33.53	21.73	16.34	23583.10
16	15.17	37.82	33.53	21.73	16.34	23583.10
17	15.18	38.85	34.37	22.03	16.39	25467.47
18	14.02	78.24	66.07	32.61	17.32	31038.51
19	15.07	45.55	39.78	23.90	16.64	28006.88
20	15.18	39.88	35.20	22.33	16.45	27422.37
21	15.18	39.63	35.00	22.26	16.43	26931.89
22	15.18	39.11	34.57	22.11	16.41	25945.85
23	15.17	37.82	33.53	21.73	16.34	23583.10
24	15.17	36.28	32.28	21.28	16.25	20879.49

Table 11: DC OPF Solution Results in SI Units for Five-Node Case - Thermal Limit Inequality Constraint Multipliers for Each Branch in Each Direction (km and mk)

		Branch km multipliers										
Hour	12	14	15	23	34	45	21	41	51	32	43	54
01	30.36	0	0	0	0	0	0	0	0	0	0	0
02	28.05	0	0	0	0	0	0	0	0	0	0	0
03	26.52	0	0	0	0	0	0	0	0	0	0	0
04	25.74	0	0	0	0	0	0	0	0	0	0	0
05	24.99	0	0	0	0	0	0	0	0	0	0	0
06	25.37	0	0	0	0	0	0	0	0	0	0	0
07	25.74	0	0	0	0	0	0	0	0	0	0	0
08	27.29	0	0	0	0	0	0	0	0	0	0	0
09	31.12	0	0	0	0	0	0	0	0	0	0	0
10	34.20	0	0	0	0	0	0	0	0	0	0	0
11	34.97	0	0	0	0	0	0	0	0	0	0	0
12	35.35	0	0	0	0	0	0	0	0	0	0	0
13	34.97	0	0	0	0	0	0	0	0	0	0	0
14	34.20	0	0	0	0	0	0	0	0	0	0	0
15	33.82	0	0	0	0	0	0	0	0	0	0	0
16	33.82	0	0	0	0	0	0	0	0	0	0	0
17	35.35	0	0	0	0	0	0	0	0	0	0	0
18	95.88	0	0	0	0	0	0	0	0	0	0	0
19	45.50	0	0	0	0	0	0	0	0	0	0	0
20	36.88	0	0	0	0	0	0	0	0	0	0	0
21	36.50	0	0	0	0	0	0	0	0	0	0	0
22	35.73	0	0	0	0	0	0	0	0	0	0	0
23	33.82	0	0	0	0	0	0	0	0	0	0	0
24	31.51	0	0	0	0	0	0	0	0	0	0	0

Table 12: DC OPF Solution Results in SI Units for Five-Node Case - Lower and Upper Production Inequality Constraint Multipliers for Each Generator

Hour	P^L_{G1}	P^L_{G2}	P^L_{G3}	P^L_{G4}	P^L_{G5}	P^U_{G1}	P^U_{G2}	P^U_{G3}	P^U_{G4}	P^U_{G5}
01	0	0	0	8.95	0	0.07	0	0	0	0
02	0	0	0	9.40	0	0.06	0	0	0	0
03	0	0	0	9.70	0	0.06	0	0	0	0
04	0	0	0	9.85	0	0.06	0	0	0	0
05	0	0	0	10.00	0	0.05	0	0	0	0
06	0	0	0	9.93	0	0.06	0	0	0	0
07	0	0	0	9.85	0	0.06	0	0	0	0
08	0	0	0	9.55	0	0.06	0	0	0	0
09	0	0	0	8.80	0	0.07	0	0	0	0
10	0	0	0	8.19	0	0.08	0	0	0	0
11	0	0	0	8.04	0	0.08	0	0	0	0
12	0	0	0	7.97	0	0.08	0	0	0	0
13	0	0	0	8.04	0	0.08	0	0	0	0
14	0	0	0	8.19	0	0.08	0	0	0	0
15	0	0	0	8.27	0	0.07	0	0	0	0
16	0	0	0	8.27	0	0.07	0	0	0	0
17	0	0	0	7.97	0	0.08	0	0	0	0
18	0	0.98	0	0	0	0	0	30.67	0	0
19	0	0	0	6.10	0	0	0	4.38	0	0
20	0	0	0	7.67	0	0.08	0	0	0	0
21	0	0	0	7.74	0	0.08	0	0	0	0
22	0	0	0	7.89	0	0.08	0	0	0	0
23	0	0	0	8.27	0	0.07	0	0	0	0
24	0	0	0	8.72	0	0.07	0	0	0	0

Table 13: DC OPF Solution Results in SI Units for Five-Node Case - Optimal Real Power Branch Flow P_{km} and Its Associated Thermal Limit P_{km}^U for Each $km \in \mathbf{BI}$

Hour	P_{12} [a]	P_{14}	P_{15}	P_{23}	P_{34}	P_{45}
01	250.00	129.65	-255.77	-100.00	-67.47	-187.82
02	250.00	126.71	-253.27	-72.93	-80.32	-184.27
03	250.00	124.77	-251.61	-55.04	-88.81	-181.93
04	250.00	123.79	-250.77	-46.02	-93.09	-180.74
05	250.00	122.83	-249.95	-37.16	-97.30	-179.58
06	250.00	123.31	-250.36	-41.59	-95.19	-180.16
07	250.00	123.79	-250.77	-46.02	-93.09	-180.74
08	250.00	125.75	-252.45	-64.07	-84.52	-183.11
09	250.00	130.61	-256.60	-108.86	-63.26	-188.98
10	250.00	134.51	-259.92	-144.80	-46.20	-193.69
11	250.00	135.49	-260.76	-153.82	-41.92	-194.87
12	250.00	135.97	-261.17	-158.25	-39.81	-195.45
13	250.00	135.49	-260.76	-153.82	-41.92	-194.87
14	250.00	134.51	-259.92	-144.80	-46.20	-193.69
15	250.00	134.03	-259.51	-140.37	-48.30	-193.11
16	250.00	134.03	-259.51	-140.37	-48.30	-193.11
17	250.00	135.97	-261.17	-158.25	-39.81	-195.45
18	250.00	98.83	-346.76	-198.62	-63.15	-175.88
19	250.00	137.64	-274.17	-180.73	-29.93	-199.96
20	250.00	137.91	-262.83	-176.14	-31.32	-197.80
21	250.00	137.43	-262.42	-171.71	-33.42	-197.22
22	250.00	136.45	-261.58	-162.69	-37.71	-196.03
23	250.00	134.03	-259.51	-140.37	-48.30	-193.11
24	250.00	131.11	-257.02	-113.46	-61.08	-189.58
	P_{12}^U	P_{14}^U	P_{15}^U	P_{23}^U	P_{34}^U	P_{45}^U
	250.00	150.00	400.00	350.00	240.00	240.00

[a] In accordance with the usual convention, the real power P_{km} flowing along a branch km is positively valued if and only if real power is flowing from node k to node m.

Table 14: Sensitivity Test Results for Three-Node Case ($\pi = 100$, Angles in Radians)

Hour	p^*_{G1}	p^*_{G2}	p^*_{G3}	δ^*_2	δ^*_3	LMP_1	LMP_2	LMP_3	minTVC
01	200.0	16.1	5.0	-0.079920	-0.109520	18.2555	18.2971	18.3239	2993.95
02	189.0	10.0	5.0	-0.080800	-0.104800	12.4441	12.4858	12.5094	2724.33
03	177.7	10.0	5.0	-0.075216	-0.097887	12.3395	12.3783	12.4005	2565.12
04	172.0	10.0	5.0	-0.072400	-0.094400	12.2867	12.3240	12.3455	2485.70
05	166.4	10.0	5.0	-0.069633	-0.090974	12.2349	12.2708	12.2915	2408.27
06	169.2	10.0	5.0	-0.071016	-0.092687	12.2608	12.2974	12.3185	2446.91
07	172.0	10.0	5.0	-0.072400	-0.094400	12.2867	12.3240	12.3455	2485.70
08	183.4	10.0	5.0	-0.078033	-0.101374	12.3923	12.4325	12.4554	2645.13
09	200.0	21.7	5.0	-0.074122	-0.107675	18.3266	18.3656	18.3941	3097.90
10	200.0	44.4	5.0	-0.050621	-0.100198	18.6149	18.6435	18.6786	3527.13
11	200.0	50.1	5.0	-0.044720	-0.098320	18.6873	18.7132	18.7500	3636.90
12	200.0	52.9	5.0	-0.041821	-0.097398	18.7229	18.7475	18.7851	3691.11
13	200.0	50.1	5.0	-0.044720	-0.098320	18.6873	18.7132	18.7500	3636.90
14	200.0	44.4	5.0	-0.050621	-0.100198	18.6149	18.6435	18.6786	3527.13
15	200.0	41.6	5.0	-0.053520	-0.101120	18.5794	18.6092	18.6435	3473.51
16	200.0	41.6	5.0	-0.053520	-0.101120	18.5794	18.6092	18.6435	3473.51
17	200.0	52.9	5.0	-0.041821	-0.097398	18.7229	18.7475	18.7851	3691.11
18	200.0	78.4	5.0	-0.015421	-0.088998	19.0468	19.0596	19.1047	4193.64
19	200.0	67.1	5.0	-0.027120	-0.092720	18.9033	18.9213	18.9631	3968.98
20	200.0	64.2	5.0	-0.030122	-0.093675	18.8664	18.8858	18.9267	3911.83
21	200.0	61.4	5.0	-0.033021	-0.094598	18.8309	18.8515	18.8916	3856.85
22	200.0	55.7	5.0	-0.038922	-0.096475	18.7585	18.7818	18.8202	3745.51
23	200.0	41.6	5.0	-0.053520	-0.101120	18.5794	18.6092	18.6435	3473.51
24	200.0	24.6	5.0	-0.071120	-0.106720	18.3634	18.4011	18.4304	3152.03

Table 15: Sensitivity Test Results for Three-Node Case ($\pi = 10$, Angles in Radians)

Hour	p^*_{G1}	p^*_{G2}	p^*_{G3}	δ^*_2	δ^*_3	LMP_1	LMP_2	LMP_3	minTVC
01	200.0	16.1	5.0	-0.079920	-0.109520	18.2929	18.2971	18.2997	2993.95
02	189.0	10.0	5.0	-0.080800	-0.104800	12.4441	12.4483	12.4507	2724.33
03	177.7	10.0	5.0	-0.075216	-0.097887	12.3395	12.3434	12.3456	2565.12
04	172.0	10.0	5.0	-0.072400	-0.094400	12.2867	12.2905	12.2926	2485.70
05	166.4	10.0	5.0	-0.069633	-0.090974	12.2349	12.2385	12.2405	2408.27
06	169.2	10.0	5.0	-0.071016	-0.092687	12.2608	12.2645	12.2666	2446.91
07	172.0	10.0	5.0	-0.072400	-0.094400	12.2867	12.2905	12.2926	2485.70
08	183.4	10.0	5.0	-0.078033	-0.101374	12.3923	12.3963	12.3986	2645.13
09	200.0	21.7	5.0	-0.074122	-0.107675	18.3617	18.3656	18.3685	3097.90
10	200.0	44.4	5.0	-0.050621	-0.100198	18.6406	18.6435	18.6470	3527.13
11	200.0	50.1	5.0	-0.044720	-0.098320	18.7106	18.7132	18.7169	3636.90
12	200.0	52.9	5.0	-0.041821	-0.097398	18.7450	18.7475	18.7513	3691.11
13	200.0	50.1	5.0	-0.044720	-0.098320	18.7106	18.7132	18.7169	3636.90
14	200.0	44.4	5.0	-0.050621	-0.100198	18.6406	18.6435	18.6470	3527.13
15	200.0	41.6	5.0	-0.053520	-0.101120	18.6062	18.6092	18.6126	3473.51
16	200.0	41.6	5.0	-0.053520	-0.101120	18.6062	18.6092	18.6126	3473.51
17	200.0	52.9	5.0	-0.041821	-0.097398	18.7450	18.7475	18.7513	3691.11
18	200.0	78.4	5.0	-0.015421	-0.088998	19.0583	19.0596	19.0641	4193.64
19	200.0	67.1	5.0	-0.027120	-0.092720	18.9195	18.9213	18.9255	3968.98
20	200.0	64.2	5.0	-0.030122	-0.093675	18.8839	18.8858	18.8899	3911.83
21	200.0	61.4	5.0	-0.033021	-0.094598	18.8495	18.8515	18.8555	3856.85
22	200.0	55.7	5.0	-0.038922	-0.096475	18.7794	18.7818	18.7856	3745.51
23	200.0	41.6	5.0	-0.053520	-0.101120	18.6062	18.6092	18.6126	3473.51
24	200.0	24.6	5.0	-0.071120	-0.106720	18.3973	18.4011	18.4040	3152.03

Table 16: Sensitivity Test Results for Three-Node Case ($\pi = 1$, Angles in Radians)

Hour	p^*_{G1}	p^*_{G2}	p^*_{G3}	δ^*_2	δ^*_3	LMP_1	LMP_2	LMP_3	minTVC
01	200.0	16.1	5.0	-0.079920	-0.109520	18.2966	18.2971	18.2973	2993.95
02	189.0	10.0	5.0	-0.080800	-0.104800	12.4441	12.4446	12.4448	2724.33
03	177.7	10.0	5.0	-0.075216	-0.097887	12.3395	12.3399	12.3401	2565.12
04	172.0	10.0	5.0	-0.072400	-0.094400	12.2867	12.2871	12.2873	2485.70
05	166.4	10.0	5.0	-0.069633	-0.090974	12.2349	12.2352	12.2354	2408.27
06	169.2	10.0	5.0	-0.071016	-0.092687	12.2608	12.2612	12.2614	2446.91
07	172.0	10.0	5.0	-0.072400	-0.094400	12.2867	12.2871	12.2873	2485.70
08	183.4	10.0	5.0	-0.078033	-0.101374	12.3923	12.3927	12.3929	2645.13
09	200.0	21.7	5.0	-0.074122	-0.107675	18.3652	18.3656	18.3659	3097.90
10	200.0	44.4	5.0	-0.050621	-0.100198	18.6432	18.6435	18.6438	3527.13
11	200.0	50.1	5.0	-0.044720	-0.098320	18.7130	18.7132	18.7136	3636.90
12	200.0	52.9	5.0	-0.041821	-0.097398	18.7473	18.7475	18.7479	3691.11
13	200.0	50.1	5.0	-0.044720	-0.098320	18.7130	18.7132	18.7136	3636.90
14	200.0	44.4	5.0	-0.050621	-0.100198	18.6432	18.6435	18.6438	3527.13
15	200.0	41.6	5.0	-0.053520	-0.101120	18.6089	18.6092	18.6095	3473.51
16	200.0	41.6	5.0	-0.053520	-0.101120	18.6089	18.6092	18.6095	3473.51
17	200.0	52.9	5.0	-0.041821	-0.097398	18.7473	18.7475	18.7479	3691.11
18	200.0	78.4	5.0	-0.015421	-0.088998	19.0595	19.0596	19.0601	4193.64
19	200.0	67.1	5.0	-0.027120	-0.092720	18.9211	18.9213	18.9217	3968.98
20	200.0	64.2	5.0	-0.030122	-0.093675	18.8856	18.8858	18.8862	3911.83
21	200.0	61.4	5.0	-0.033021	-0.094598	18.8513	18.8515	18.8519	3856.85
22	200.0	55.7	5.0	-0.038922	-0.096475	18.7815	18.7818	18.7822	3745.51
23	200.0	41.6	5.0	-0.053520	-0.101120	18.6089	18.6092	18.6095	3473.51
24	200.0	24.6	5.0	-0.071120	-0.106720	18.4007	18.4011	18.4014	3152.03

Table 17: Sensitivity Test Results for Three-Node Case ($\pi = 0.1$, Angles in Radians)

Hour	p^*_{G1}	p^*_{G2}	p^*_{G3}	δ^*_2	δ^*_3	LMP_1	LMP_2	LMP_3	minTVC
01	200.0	16.1	5.0	-0.079920	-0.109520	18.2970	18.2971	18.2971	2993.95
02	189.0	10.0	5.0	-0.080800	-0.104800	12.4441	12.4442	12.4442	2724.33
03	177.7	10.0	5.0	-0.075216	-0.097887	12.3395	12.3395	12.3396	2565.12
04	172.0	10.0	5.0	-0.072400	-0.094400	12.2867	12.2868	12.2868	2485.70
05	166.4	10.0	5.0	-0.069633	-0.090974	12.2349	12.2349	12.2349	2408.27
06	169.2	10.0	5.0	-0.071016	-0.092687	12.2608	12.2608	12.2608	2446.91
07	172.0	10.0	5.0	-0.072400	-0.094400	12.2867	12.2868	12.2868	2485.70
08	183.4	10.0	5.0	-0.078033	-0.101374	12.3923	12.3923	12.3923	2645.13
09	200.0	21.7	5.0	-0.074122	-0.107675	18.3656	18.3656	18.3656	3097.90
10	200.0	44.4	5.0	-0.050621	-0.100198	18.6434	18.6435	18.6435	3527.13
11	200.0	50.1	5.0	-0.044720	-0.098320	18.7132	18.7132	18.7133	3636.90
12	200.0	52.9	5.0	-0.041821	-0.097398	18.7475	18.7475	18.7475	3691.11
13	200.0	50.1	5.0	-0.044720	-0.098320	18.7132	18.7132	18.7133	3636.90
14	200.0	44.4	5.0	-0.050621	-0.100198	18.6434	18.6435	18.6435	3527.13
15	200.0	41.6	5.0	-0.053520	-0.101120	18.6092	18.6092	18.6092	3473.51
16	200.0	41.6	5.0	-0.053520	-0.101120	18.6092	18.6092	18.6092	3473.51
17	200.0	52.9	5.0	-0.041821	-0.097398	18.7475	18.7475	18.7475	3691.11
18	200.0	78.4	5.0	-0.015421	-0.088998	19.0596	19.0596	19.0597	4193.64
19	200.0	67.1	5.0	-0.027120	-0.092720	18.9213	18.9213	18.9213	3968.98
20	200.0	64.2	5.0	-0.030122	-0.093675	18.8858	18.8858	18.8858	3911.83
21	200.0	61.4	5.0	-0.033021	-0.094598	18.8515	18.8515	18.8516	3856.85
22	200.0	55.7	5.0	-0.038922	-0.096475	18.7817	18.7818	18.7818	3745.51
23	200.0	41.6	5.0	-0.053520	-0.101120	18.6092	18.6092	18.6092	3473.51
24	200.0	24.6	5.0	-0.071120	-0.106720	18.4011	18.4011	18.4011	3152.03

Table 18: Sensitivity Test Results for Three-Node Case ($\pi = 0.01$, Angles in Radians)

Hour	p^*_{G1}	p^*_{G2}	p^*_{G3}	δ^*_2	δ^*_3	LMP_1	LMP_2	LMP_3	minTVC
01	200.0	16.1	5.0	-0.079920	-0.109520	18.2971	18.2971	18.2971	2993.95
02	189.0	10.0	5.0	-0.080800	-0.104800	12.4441	12.4441	12.4441	2724.33
03	177.7	10.0	5.0	-0.075216	-0.097887	12.3395	12.3395	12.3395	2565.12
04	172.0	10.0	5.0	-0.072400	-0.094400	12.2867	12.2867	12.2867	2485.70
05	166.4	10.0	5.0	-0.069633	-0.090974	12.2349	12.2349	12.2349	2408.27
06	169.2	10.0	5.0	-0.071016	-0.092687	12.2608	12.2608	12.2608	2446.91
07	172.0	10.0	5.0	-0.072400	-0.094400	12.2867	12.2867	12.2867	2485.70
08	183.4	10.0	5.0	-0.078033	-0.101374	12.3923	12.3923	12.3923	2645.13
09	200.0	21.7	5.0	-0.074122	-0.107675	18.3656	18.3656	18.3656	3097.90
10	200.0	44.4	5.0	-0.050621	-0.100198	18.6435	18.6435	18.6435	3527.13
11	200.0	50.1	5.0	-0.044720	-0.098320	18.7132	18.7132	18.7132	3636.90
12	200.0	52.9	5.0	-0.041821	-0.097398	18.7475	18.7475	18.7475	3691.11
13	200.0	50.1	5.0	-0.044720	-0.098320	18.7132	18.7132	18.7132	3636.90
14	200.0	44.4	5.0	-0.050621	-0.100198	18.6435	18.6435	18.6435	3527.13
15	200.0	41.6	5.0	-0.053520	-0.101120	18.6092	18.6092	18.6092	3473.51
16	200.0	41.6	5.0	-0.053520	-0.101120	18.6092	18.6092	18.6092	3473.51
17	200.0	52.9	5.0	-0.041821	-0.097398	18.7475	18.7475	18.7475	3691.11
18	200.0	78.4	5.0	-0.015421	-0.088998	19.0596	19.0596	19.0596	4193.64
19	200.0	67.1	5.0	-0.027120	-0.092720	18.9213	18.9213	18.9213	3968.98
20	200.0	64.2	5.0	-0.030122	-0.093675	18.8858	18.8858	18.8858	3911.83
21	200.0	61.4	5.0	-0.033021	-0.094598	18.8515	18.8515	18.8515	3856.85
22	200.0	55.7	5.0	-0.038922	-0.096475	18.7818	18.7818	18.7818	3745.51
23	200.0	41.6	5.0	-0.053520	-0.101120	18.6092	18.6092	18.6092	3473.51
24	200.0	24.6	5.0	-0.071120	-0.106720	18.4011	18.4011	18.4011	3152.03

Table 19: Sensitivity Test Results for Three-Node Case - Cross Comparison for Sum of Squared Voltage Angle Differences for $\pi = 100, 10, 1, 0.1, 0.01$, Angles in Radians

Hour	$SSVAD_{100}$ [a]	$SSVAD_{10}$	$SSVAD_{1}$	$SSVAD_{0.1}$	$SSVAD_{0.01}$	MaxAD[b]
01	0.019257997	0.019257997	0.019257997	0.019257997	0.019257997	8.10E-15
02	0.018087680	0.018087680	0.018087680	0.018087680	0.018087680	4.16E-14
03	0.015753349	0.015753349	0.015753349	0.015753349	0.015753349	3.95E-14
04	0.014637120	0.014637120	0.014637120	0.014637120	0.014637120	3.83E-14
05	0.013580482	0.013580482	0.013580482	0.013580482	0.013580482	3.71E-14
06	0.014103844	0.014103844	0.014103844	0.014103844	0.014103844	3.77E-14
07	0.014637120	0.014637120	0.014637120	0.014637120	0.014637120	3.83E-14
08	0.016910662	0.016910662	0.016910662	0.016910662	0.016910662	4.05E-14
09	0.018213892	0.018213892	0.018213892	0.018213892	0.018213892	7.30E-15
10	0.015059898	0.015059898	0.015059898	0.015059898	0.015059898	4.50E-15
11	0.014539661	0.014539661	0.014539661	0.014539661	0.014539661	3.80E-15
12	0.014324057	0.014324057	0.014324057	0.014324057	0.014324057	3.80E-15
13	0.014539661	0.014539661	0.014539661	0.014539661	0.014539661	3.80E-15
14	0.015059898	0.015059898	0.015059898	0.015059898	0.015059898	4.50E-15
15	0.015355405	0.015355405	0.015355405	0.015355405	0.015355405	4.70E-15
16	0.015355405	0.015355405	0.015355405	0.015355405	0.015355405	4.70E-15
17	0.014324057	0.014324057	0.014324057	0.014324057	0.014324057	3.80E-15
18	0.013571891	0.013571891	0.013571891	0.013571891	0.013571891	1.19E-14
19	0.013635853	0.013635853	0.013635853	0.013635853	0.013635853	1.50E-14
20	0.013721393	0.013721393	0.013721393	0.013721393	0.013721393	1.63E-14
21	0.013830775	0.013830775	0.013830775	0.013830775	0.013830775	1.76E-14
22	0.014134773	0.014134773	0.014134773	0.014134773	0.014134773	1.99E-14
23	0.015355405	0.015355405	0.015355405	0.015355405	0.015355405	4.70E-15
24	0.017714573	0.017714573	0.017714573	0.017714573	0.017714573	7.00E-15

[a]Sum of squared voltage angle differences for a specific choice of π, where π is specified to be 100, 10, 1, 0.1 or 0.01. More precisely, SSVAD = $\sum_{km \in \mathbf{BI}} [\delta_k^* - \delta_m^*]^2$

[b]Maximum absolute difference between any two SSVAD values

Table 20: Sensitivity Test Results for Five-Node Case - Cross Comparison for Sum of Squared Voltage Angle Differences for $\pi = 100, 10, 1, 0.1, 0.01$, Angles in Radians

Hour	$SSVAD_{100}$	$SSVAD_{10}$	$SSVAD_{1}$	$SSVAD_{0.1}$	$SSVAD_{0.01}$	MaxAD
01	0.010386061	0.010386162	0.010386172	0.010386173	0.010386173	1.12E-07
02	0.010307655	0.010307759	0.010307769	0.010307770	0.010307771	1.16E-07
03	0.010283485	0.010283591	0.010283602	0.010283603	0.010283603	1.18E-07
04	0.010279443	0.010279550	0.010279561	0.010279562	0.010279562	1.19E-07
05	0.010280962	0.010281070	0.010281081	0.010281082	0.010281082	1.20E-07
06	0.010279593	0.010279701	0.010279712	0.010279713	0.010279713	1.20E-07
07	0.010279443	0.010279550	0.010279561	0.010279562	0.010279562	1.19E-07
08	0.010292874	0.010292979	0.010292989	0.010292990	0.010292991	1.17E-07
09	0.010422608	0.010422708	0.010422718	0.010422719	0.010422719	1.11E-07
10	0.010625778	0.010625874	0.010625884	0.010625885	0.010625885	1.07E-07
11	0.010690587	0.010690682	0.010690691	0.010690692	0.010690692	1.05E-07
12	0.010724577	0.010724671	0.010724680	0.010724681	0.010724681	1.05E-07
13	0.010690587	0.010690682	0.010690691	0.010690692	0.010690692	1.05E-07
14	0.010625778	0.010625874	0.010625884	0.010625885	0.010625885	1.07E-07
15	0.010595866	0.010595962	0.010595972	0.010595973	0.010595973	1.07E-07
16	0.010595866	0.010595962	0.010595972	0.010595973	0.010595973	1.07E-07
17	0.010724577	0.010724671	0.010724680	0.010724681	0.010724681	1.05E-07
18	0.009870395	0.009870652	0.009870678	0.009870680	0.009870681	2.86E-07
19	0.010980723	0.010980723	0.010980723	0.010980723	0.010980722	6.60E-10
20	0.010875114	0.010875206	0.010875215	0.010875216	0.010875216	1.03E-07
21	0.010835704	0.010835797	0.010835806	0.010835807	0.010835807	1.03E-07
22	0.010759863	0.010759957	0.010759967	0.010759968	0.010759968	1.04E-07
23	0.010595866	0.010595962	0.010595972	0.010595973	0.010595973	1.07E-07
24	0.010443596	0.010443696	0.010443705	0.010443707	0.010443707	1.10E-07